EJECTOR EFFECTS ON A SUPERSONIC NOZZLE AT LOW ALTITUDE AND MACH NUMBER

THESIS

Christopher A. Seaver
Captain, USAF

AFIT/GAE/AA/88D-33

DEPARTMENT OF THE AIR FORCE
AIR UNIVERSITY
AIR FORCE INSTITUTE OF TECHNOLOGY
Wright-Patterson Air Force Base, Ohio

AFIT/GAE/AA/88D-33

EJECTOR EFFECTS ON A SUPERSONIC NOZZLE AT LOW ALTITUDE AND MACH NUMBER

THESIS

Christopher A. Seaver
Captain, USAF

AFIT/GAE/AA/88D-33

Approved for public release; distribution unlimited

AFIT/GAE/AA/88D-33

EJECTOR EFFECTS ON A SUPERSONIC NOZZLE AT LOW ALTITUDE AND MACH NUMBER

THESIS

Presented to the Faculty of the School of Engineering

of the Air Force Institute of Technology

Air University

In Partial Fulfillment of the

Requirements for the Degree of

Master of Science in Aeronautical Engineering

Christopher A. Seaver

Captain, USAF

December 1988

Approved for public release; distribution unlimted

Preface

This topic was selected with three goals in mind. First, with my previous background strongly based in the propulsion area, this study provided a medium to increase my awareness of the subject. Next, being a pilot, I hoped to find an area which I had gained some experience previously. My experience with Air Training Command flying T-38s and teaching the engine systems of that aircraft to new pilot training students led me toward a propulsive system thesis. Finally, since I will have to remain on the ground for a few more years, I hope to gain more knowledge for future engine technology improvements so that I may understand what I may one day be using to fly.

The successful completion of this project was solely due to the guidance and help of my advisor, Dr. W. C. Elrod. While continuing to look for direction and answers during my research, Dr. Elrod was always there with the direction, the answer, or an encouraging word that something would turn up soon. Also, I must express my thanks to Lt Col Jack Mattingly. From the early days of my study at the Air Force Academy to the final long nights spent completing this thesis, no one instructor has done more for my understanding of aircraft and rocket propulsion than him. Additionally, Lt Col Paul King and Dr. M. Franke each provided important insight for this project.

The technicians from the department also deserve much for their support. Messrs. Nick Yardich, Jay Anderson, Leroy Cannon, Gerald Hild, and Tim Major were invaluable in their efforts to support my experiment. Mr. John Brohas from the AFIT fabrication shop deserves a great deal of credit for making a masterpiece of a test section from a collection of rough sketches. Also, Capt Tom Hotchkiss deserves a great deal of thanks for the use of his VCR system for an extended period of time.

Finally, this work must be dedicated to my family. My wife Lyn and my three sons Craig, Ryan, and Chad have been my strength throughout this long, yet satisfying experience. Their support and God's grace guided me through it all.

Christopher A. Seaver

Table of Contents

List of Figures

Figure Page

List of Tables

List of Symbols

Symbols	Definition
A	area (in^2)
AFIT	Air Force Institute of Technology
cm	centimeter
d	density (lbm/ft^3, $slugs/ft^3$)
D.C.	direct current (volts)
F	thrust (lbf)
ft	feet
g_c	conversion factor ($lbm\text{-}ft/lbf\text{-}sec^2$)
g_o	acceleration of gravity (ft^2/sec)
Hg	mercury
HP	Hewlett Packard
IB	interface bus
in	inches
I_{sp}	specific impulse (sec)
k	specific heat ratio
L	mixing chamber length (in)
lbf	pounds force
lbm	pounds mass
M	Mach number
MFP	mass flow parameter ($lbm\text{-}\sqrt{°R}/lbf\text{-}s$)
m	mass flow rate (lbm/sec)
mm	millimeter
P	pressure (psi)
psi	pounds force per inch squared

Symbols	Definition
psia	psi absolute
psig	psi gage
P1	rocket plenum pressure (psia)
P2	wall pressure #1 (psia)
P3	wall pressure #2 (psia)
P4	wall pressure #3 (psia)
P5	wall pressure #4 (psia)
P6	wall pressure #5 (psia)
P7	wall pressure #6 (psia)
P8	ejector plenum pressure (psia)
P9	vacuum tank or back pressure (psia)
R	gas constant (ft-lbf/lbm-°R)
sec	seconds
U	velocity (feet per second)
φ	thrust augmentation ratio
Σ	summation

Subscripts	Definition
A	air or ambient
C	chamber
E	exit
F	fuel
T	total
W	wall
1	primary flow
2	secondary flow
3	mixing chamber flow

Abstract

This research involves the study of ejector effects on a supersonic nozzle. A blowdown wind tunnel was used to simulate the launch of an ejector rocket to determine possible thrust augmentation capabilities of such a design. Pressure measurements were made along the mixing chamber during the 42 separate runs which were used to select a specified profile to study the effects the flow has on wall pressures and rocket thrust.

Primary airflow was directed to the primary rocket nozzle designed for Mach 3.09. Secondary airflow was directed to a sonic ejector which was adjusted to simulate vehicle Mach number. A vacuum tank was used to provide the environment simulating a "reverse" trajectory of a launch.

Results of this investigation show a potential increase in thrust based on a one-dimensional math model designed to reflect the flow within the mixing chamber. Wall pressures are generally higher at lower altitudes and decrease as altitude increases. Possible thrust benefits that may occur due to these higher wall pressures must be balanced by structural problems that may occur due to the oscillatory nature of the flow. Geometry and magnitude of the ejector are critical to the potential thrust augmentation of the rocket due to the tremendous turbulence that can develop just beyond the primary nozzle exit plane.

EJECTOR EFFECTS ON A SUPERSONIC NOZZLE AT LOW ALTITUDE AND MACH NUMBER

I. Introduction

As the 21st century approaches, the need for a single-stage-to orbit fully reusable flight vehicle is becoming more evident. With the return of the space shuttle Discovery to orbit, the United States can now begin to once again take up the idea of a permanently manned space station. Such a project would require a transportation device much more fiscally sound than the shuttle. A single-stage-to-orbit vehicle would be required to make frequent missions for resupply, personnel rotation, and overall station support.

Previous AFIT studies by Moran (1), Rodgers (2), Maxwell (3), and Wesling (4) examined the plume interactions and performance characteristics of various rocket ramjet clusters. They showed such systems have potential as a combined propulsion system to power a vehicle such as the National Aero Space Plane (NASP). One drawback mentioned and which must still be considered is the physical size and weight added to shroud such a cluster may override any thrust improvements. While the high specific impulse of an air-breathing ramjet may benefit the high thrust-to-weight but low specific impulse capabilities of most rockets, this capability does not occur until high altitudes and higher

Mach numbers (greater than Mach 3) where ramjets are most effective. The possibility exists for the ramjet system to function in conjunction with the rocket engine as an ejector system to provide additional thrust performance at low altitudes (less than 50,000 feet) and lower Mach numbers (less than 2) without significant additional hardware. If the combined propulsive system could improve performance through a large part of the launch envelope of a rocket vehicle, it could lead toward the goal of a single-stage-to-orbit vehicle.

Objectives

As mentioned, the most recent studies in this area have concentrated on the rocket ramjet performance in the high altitude and Mach number envelope. This research is designed to lay the groundwork for long term study of rocket ejector performance in the low altitude and Mach number envelope. Specifically, the objectives are as follows:

1. To experimentally examine the wall pressures through the constant area mixing chamber of the system,

2. To evaluate the changes in these pressures as vehicle speed and altitude is changed,

3. To evaluate the effect of secondary mass flow changes by varying the area of the throat of the ejector,

4. To determine the changes which occur as the location of the nozzle exit and ejector throat planes vary.

Scope

While this study could be considered a follow on to the work of Moran (1), Rodgers (2), Maxwell (3), and Wesling (4), it really marks a new direction in this area at AFIT. This is the beginning of an investigation of ejector effects on rockets and will allow a study of the transition between the ejector and the ramjet within the same propulsion system.

This study will concentrate on the differences between the high altitude benefits that have been seen in the previous studies using ramjets and the potential benefits an ejector might provide at low altitude. Wall pressure studies began by Rodgers (2) will be expanded to a farther distance down the mixing chamber and with back pressure up to approximately standard sea level pressure.

Approach

The approach taken in this study was to use a two-dimensional model for which one rocket nozzle and two possible ejector systems were developed. Two-dimensional flow was maintained by using plexiglass sidewalls downstream of the nozzle exit planes. The rocket nozzle was designed for Mach 3.09 using the method of characteristics as in Shapiro (5:462-528). The first system had the mixing chamber blocks designed to allow a secondary flow throat of 0.1 inch and the second system was similar but with a throat dimension of 0.2 inch. With each system, the blocks could

be adjusted fore or aft up to 0.5 inches in any increment desired to vary the throat locations.

A typical launch schedule shown in Figure 1 suggests the rocket velocity increases slowly up to Mach 1.5-2.0 through 40,000-50,000 feet (6:53). Each set was tested with a rocket chamber pressure of approximately 110 psia. The ejector secondary flow source pressure was adjusted between 15 psia and 35 psia to represent changes in ramjet inlet flow conditions which change with vehicle altitude and Mach number.

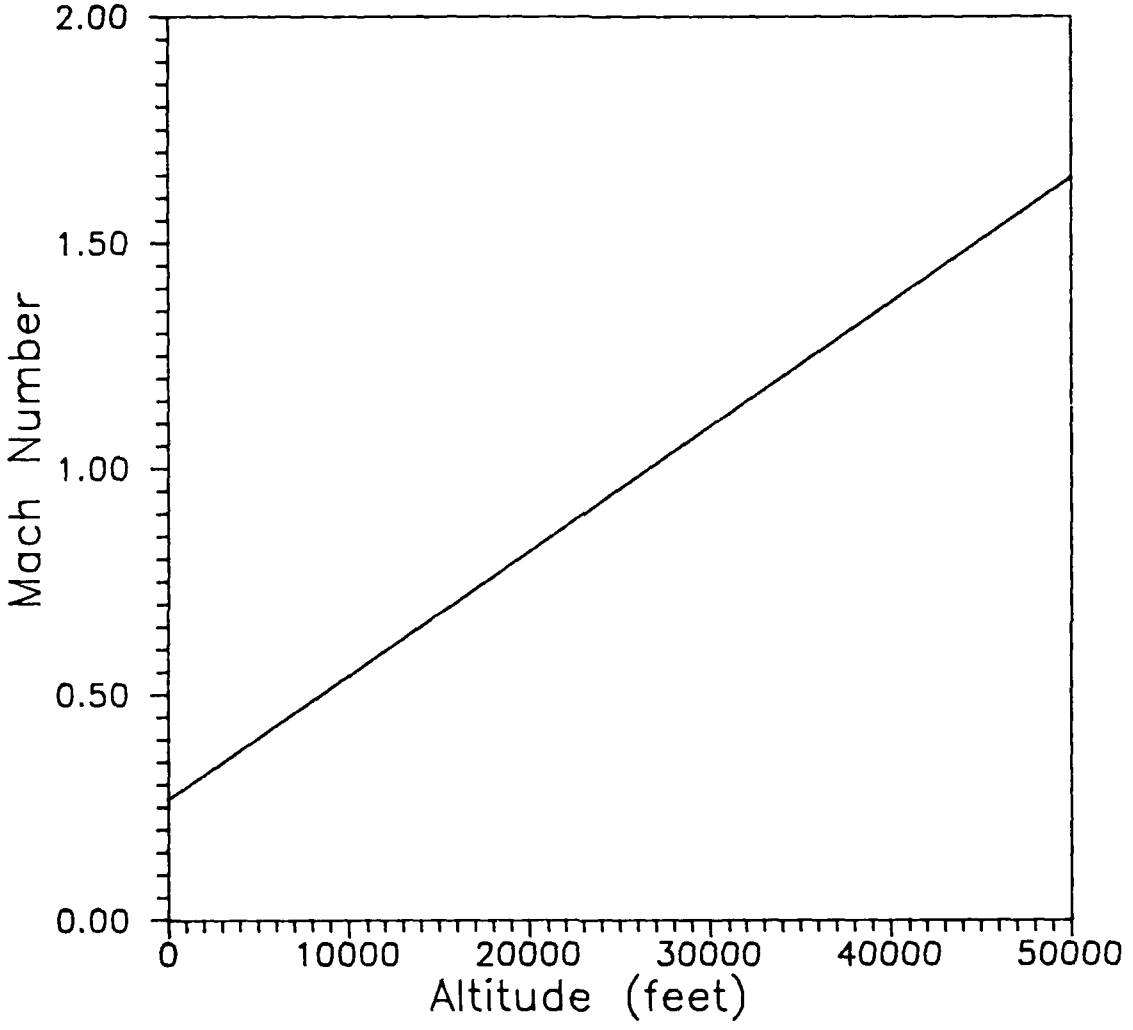

Figure 1. Typical Space Shuttle Launch Profile (6:53)

II. Theory

Rockets

Rocket propulsion force can be calculated by using the one-dimensional momentum equation which results in

$$F = mU_E + (P_E - P_A)A_E \qquad (1)$$

where

F = thrust (lbf)

m = mass flow rate (slugs/sec)

U_E = nozzle exit plane exhaust velocity (ft/sec)

P_E = nozzle exit plane pressure (lbf/in^2)

P_A = local ambient pressure (lbf/in^2)

A_E = nozzle exit plane area (in^2)

It is apparent that thrust consists of two parts. The first term is the rate of momentum transfer. The major reason for the large propulsive force of a rocket is the product of the large mass flows of propellant being exhausted and the high exit velocity. The second term is the pressure thrust. While this is relatively small compared to the momentum transfer, engine designers are very concerned with this term. Note that this term could be positive or negative depending on the designed operating altitude of the nozzle. Most rocket nozzles are therefore designed to spend most of their operation where P_E is larger than P_A to reduce the pressure drag losses which occur at the lower altitudes when $P_A > P_E$ (7:37).

The three operating conditions of a nozzle are shown in Figure 2 (8:8). Upon takeoff the rocket is initially in the overexpanded region ($P_a > P_e$) which results in the pressure drag discussed previously. The pressure differential at the nozzle exit creates an oblique shock pattern to adjust these pressures and the exhaust jet contracts downstream (9:410-411, 1:3). An example of the change from the initial condition at sea level with pressure drag to the condition at high altitude with pressure thrust can be seen in the Space Shuttle main engine which has a thrust of 470,000 lbf in a vacuum (or very high altitude) and only 375,000 lbf at sea level (1:3). As the rocket climbs it passes through the design-expansion point where $P_e = P_a$. This optimal situation could only exist at one altitude for a fixed rocket chamber pressure, P_c, unless a variable exit geometry nozzle could be developed or simulated (4:7). Such a system would undoubtedly increase weight and complexity of the nozzle and reduce any possible gains.

While creating the aforementioned positive pressure thrust, the physical results are expansion waves generated from the exit plane of the nozzle and propagated outward. The waves extend outward until interacting with a boundary which will cause a compression wave to turn the flow back in the original direction until meeting another pressure wave. This series of expansions and compressions, like the ones in the overexpanded region, form the familiar diamond-shape exhaust highly visible from a rocket nozzle.

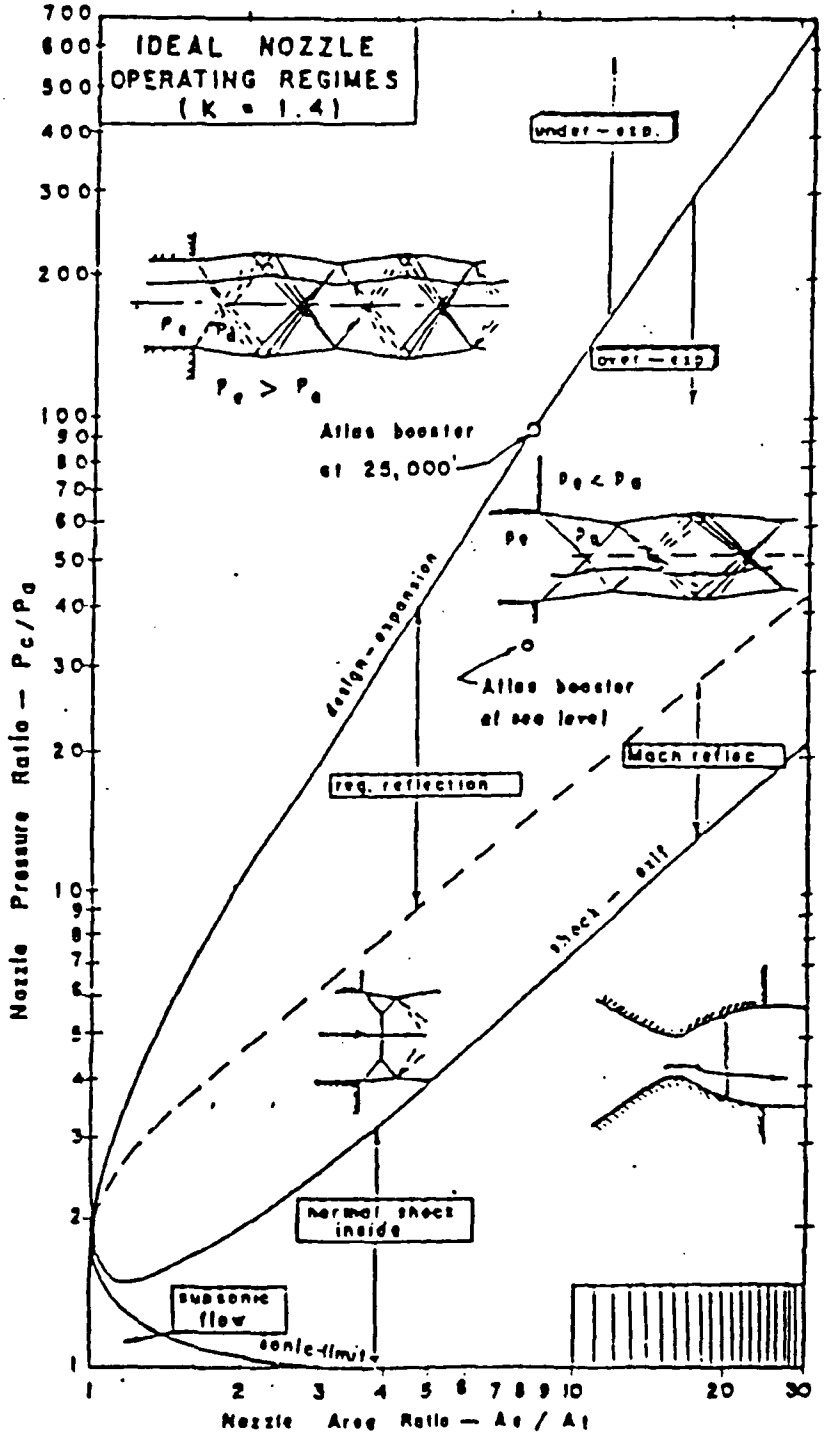

FIGURE 2. NOZZLE OPERATING DIAGRAM (8:8)

While the large thrust force is apparent in rockets, the tradeoff comes in the form of a low specific impulse, I_{sp}. Recall

$$I_{sp} = \frac{Fg_c}{\dot{m}_f g_o} \qquad (2)$$

where

I_{sp} = specific impulse (sec)

$\dot{m}_f$ = fuel mass flow rate (lbm fuel/sec)

g_c = conversion factor

= 32.174 (lbm-ft)/(lbf-sec^2)

g_o = acceleration of gravity

= 32.174 ft/sec^2

The large F is paid for with a high value of $\dot{m}_f$. Previous studies by Maxwell (3) and Wesling (4) have emphasized the possible improvements in resultant overall specific impulse that may be seen by using a ramjet with its high specific impulse in combination with the rocket engine. The hardware that would need to be added would only be useful as a ramjet at high flight speed. The hope is that it can be used as an ejector to augment thrust at the lower speeds.

Ejectors

An ejector is a device used for many different functions from jet engines to lasers. Whatever the medium, its primary purpose in propulsion is to provide thrust augmentation. The thrust augmentation is measured by

$$\varphi = \frac{d_2 A_2 U_2^2}{d_1 A_1 U_1^2} \qquad (3)$$

where

φ = thrust augmentation ratio

A_2 = mixing chamber exit area (in^2)

U_2 = mixing chamber exit velocity (ft/sec)

d_2 = mixing chamber exit density ($slugs/ft^3$)

A_1 = primary nozzle exit area (in^2)

U_1 = primary nozzle exit velocity (ft/sec)

d_1 = primary nozzle exit density ($slugs/ft^3$)

It should be apparent that if the ejector-rocket can increase the system momentum over the primary rocket nozzle momentum (and thus have $\varphi>1$), an increase in the momentum transfer from the rocket thrust equation should occur. While an accounting for the ejector-rocket inlet flow conditions which are configuration dependent must still be considered, the increase of momentum transfer across the system exit plane is the main reason for consideration of an ejector-rocket configuration.

Combined Ejector-Rocket Operation

Study in this area has been going on for several decades. Early work started by Keenan and Neumann (10) used a simple approach to break the theory down to its basic parts, while a recent study by Amatucci, Dutton, and Addy (11) was prompted by their work in high-energy chemical and gasdynamic lasers.

The purpose of an ejector in rocket operation would be for thrust augmentation. Theoretical work and study in this area requires the determination of exit static pressure of the combined ejector-rocket to compare with a standard rocket exit pressure. Additionally, the effects on the momentum flux by the addition of the ejector must be evaluated.

In 1981, Dutton, Mikkelsen, and Addy (12) did a parametric study showing the effects of several variables on pressure recovery and thus exit Mach number.

> ...it is seen that, in terms of increased compression ratios for a given primary-to-secondary mass flow ratio, the ejector pumping performance is only weakly dependent on the inlet primary Mach number, moderately dependent on the specific heat and entrance area ratios, and strongly dependent on the secondary inlet Mach number and the stagnation temperature and molecular weight ratios. (12:1396)

Likewise, ejector performance was studied by Alperin (13) for several variations of ejectors and primary engine sources. He concludes the mixing nature of the primary and induced flows has two distinct solutions which are dependent upon the resultant Mach number of the mixed flow. His final analysis, based on the information from Figure 3 for ejector-rocket possibilities is as follows:

> Performance is good at high flight speeds under all design conditions, particularly when the ejector is designed under the second solution. As indicated, subsonic mixing provides superior performance to that with supersonic mixing. It is important to note that at low speeds, the thrust augmentation of this system is extremely large provided the design configuration is that which corresponds to the second solution with subsonic mixing. (13:46)

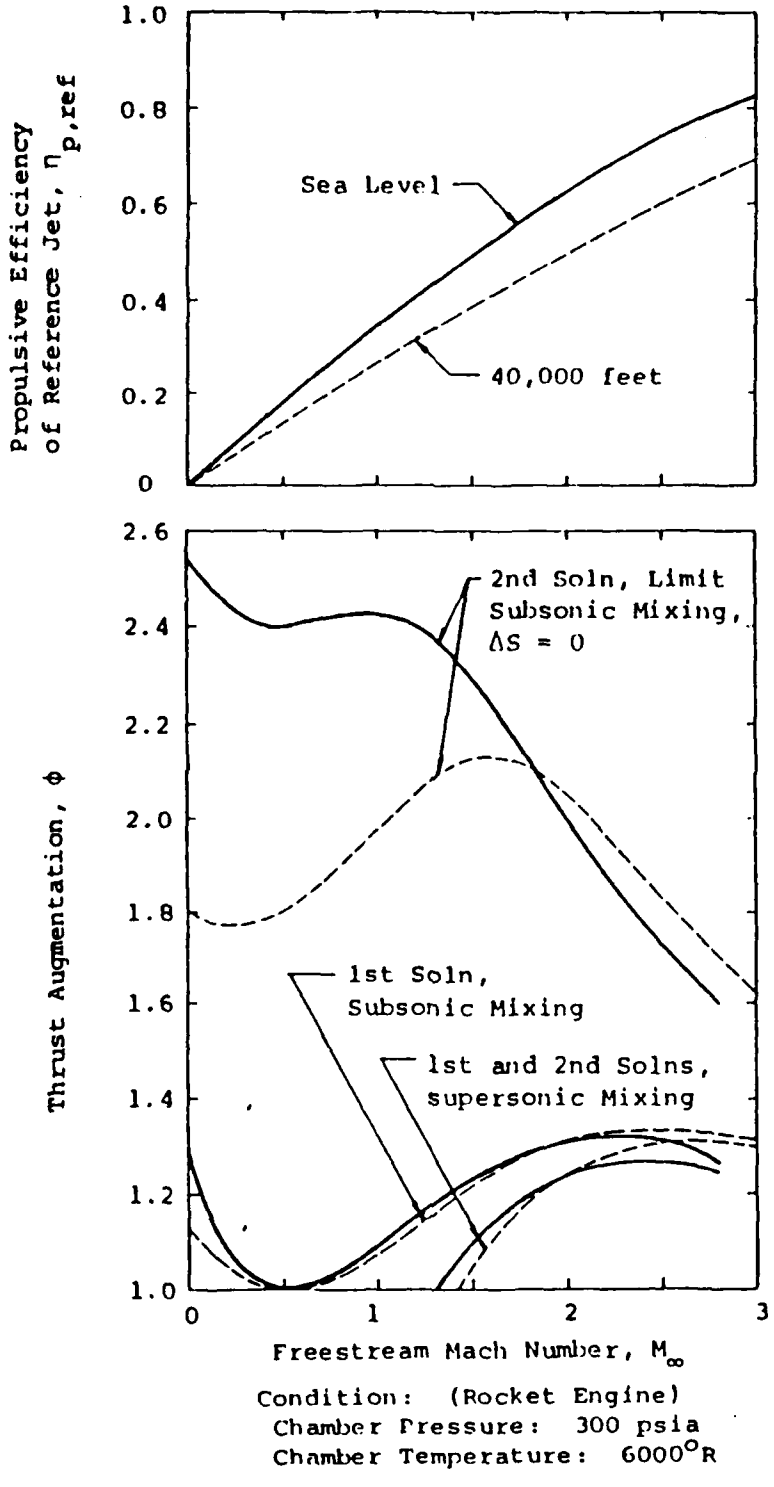

FIGURE 3. THRUST AUGMENTATION FOR ROCKET/EJECTORS (13:47)

III. Experimental Apparatus

The purpose of this study is to determine the possibilities of using the overexpanded rocket exhaust from sea level up through the nozzle design point to establish an ejector configuration for thrust augmentation.

This investigation was accomplished using the AFIT blowdown wind tunnel. The tunnel, vacuum tank, and air supply are all components of the flow system. The two-dimensional test sections and nozzles specifically designed for this study were placed inside the vacuum tank for the runs. The variations of the secondary flow throat with separate configurations made up the 42 separate runs to simulate operating conditions over a typical vehicle launch profile. Pressure transducers were installed in the mixing chamber, stilling chamber, and vacuum tank to measure operating conditions and pressure variations associated with the simulated ejector-rocket performance. Additionally, the test sections were constructed with plexiglass side plates to allow schlieren flow visualization.

Flow System

Compressed air was supplied at 110 psia and room temperature to the blowdown facility. This air was used to supply the rocket nozzle as well as the secondary flow for the purpose of simulating the possible flight conditions the ejector-rocket might encounter. Particulates and moisture

were removed from the air by a combined filter system. First, a cyclone separator used centrifugal force to remove a great deal of the moisture and solid particles. Then, a paper filter was placed just upstream of the test section to remove any remaining particulates and moisture. The cyclone separator was emptied before and after each run, and the paper filters were changed at least bimonthly to ensure proper condition and operation.

The compressed air was fed to a 3 inch diameter line which split just downstream of a manually operated disk valve. One path fed directly to the ejector-rocket primary nozzle plenum while the other went to the secondary flow plenum. The rocket nozzle was continuously supplied with the air at 110 psia. The secondary flow was regulated in several ways. First, a Grove regulator and dome valve were used to adjust the amount of pressure entering the ejector system. Two gate valves were placed just downstream of the dome valve. These valves were used to simulate the possibility of the ejector secondary air coming from the surrounding atmosphere during static rocket engine operation (like launch conditions), or be pressurized from a ram source through the ramjet inlet when the vehicle is in motion. The flow system is illustrated in Figure 4.

The test sections containing the nozzle and ejectors were installed between the air source and the 580 ft^3 vacuum chamber. Three vacuum pumps reduced the pressure in the chamber to approximately 0.1 psia. Upon receiving the flow

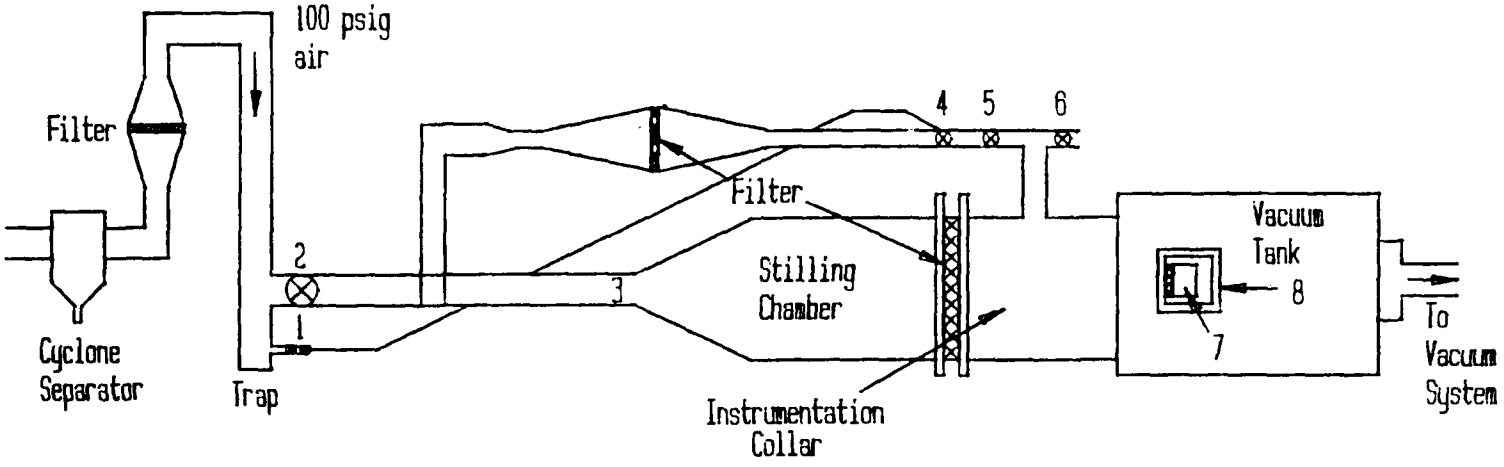

1. Grove Regulator
2. Hand Operated Valve
3. Rocket Nozzle Air Flow
4. Ejector Flow Control (Dome Valve)
5. Secondary Flow Cutoff Valve
6. Atmospheric Flow Control Valve
7. Test Section
8. Optical Window

Figure 4. Blowdown Wind Tunnel Flow System

from the supply system, the pressure in the vacuum tanks would rise simulating a "reverse trajectory" of the rocket (i.e., going from high altitude to low instead of the normal profile). An additional vacuum pump was used to establish a reference pressure of approximately 1 mm Hg absolute for the gage pressure transducers used in the test section and the vacuum tank. By using this low pressure and ensuring the transducers were "zeroed-out" on the voltage converter, the pressures could be considered absolute.

Finally, the vacuum tank has a 15 cm by 15 cm square optical quality glass window to allow schlieren photography for still or video pictures.

Test Sections

A simulated rocket nozzle was placed at the centerline of the structure exhausting into a shroud-type ejector with walls on each side of the nozzle as shown schematically in Figure 5. The section was built so the position of the primary flow exit plane could be placed up to one-half inch into or forward of the mixing chamber in any smaller increment desired. Additionally, the size of the secondary flow throat can be set at 0.1 or 0.2 inch (see Figures 6 and 7 for these variations). Each ejector mixing region configuration was designed to place up to eleven pressure transducers down the chamber; for this investigation, only six transducers were used along the top wall. The flow visualization indicated that symmetry exists within the

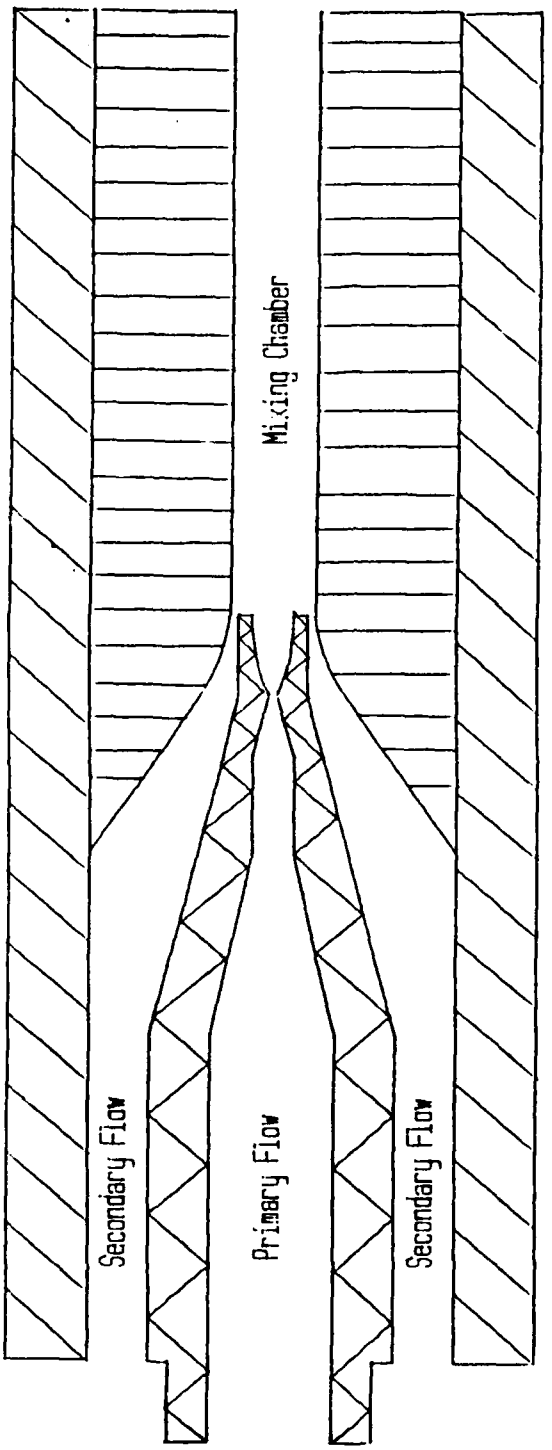

Figure 5. Test Section Cross-Section

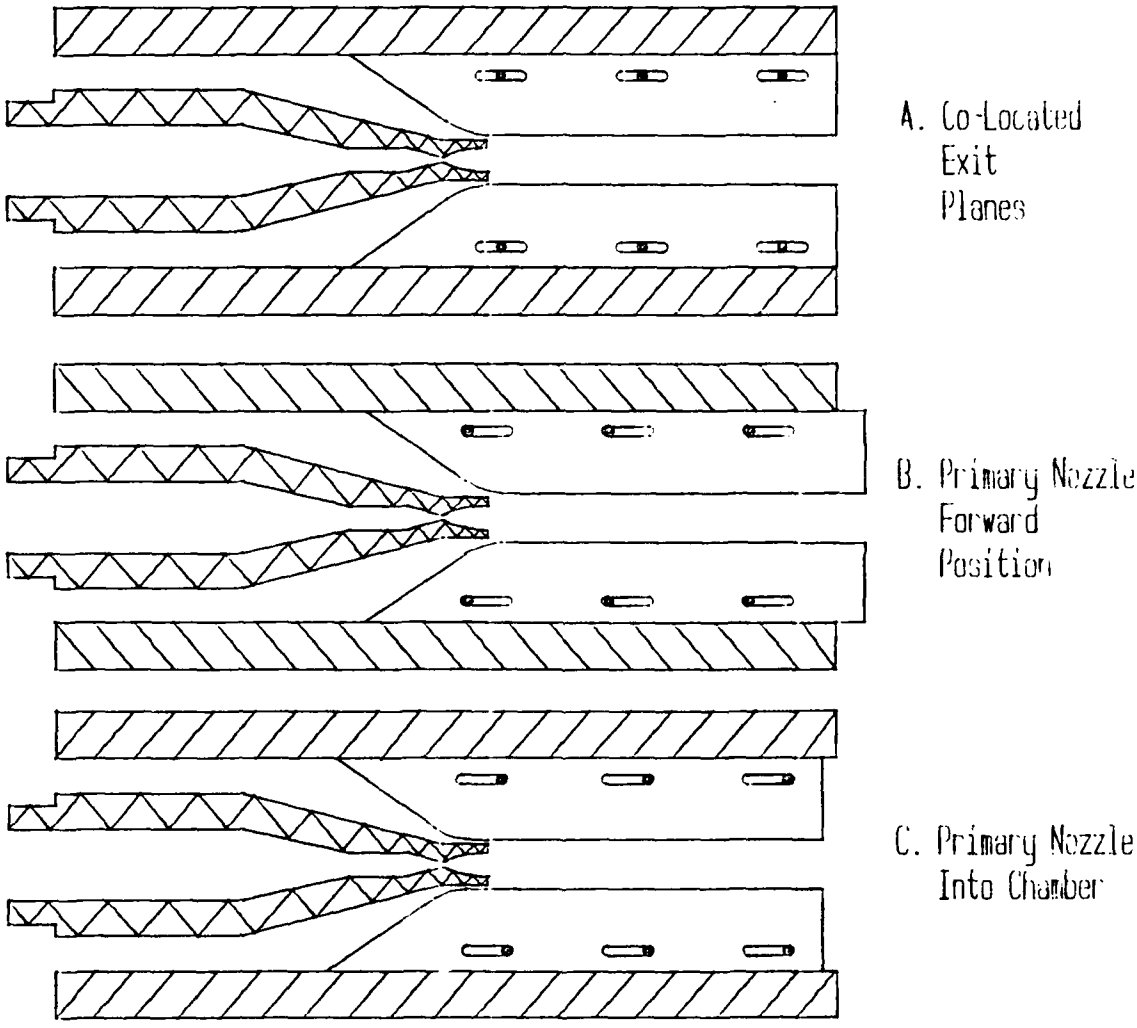

FIGURE 6. VARIATIONS OF EXIT PLANE POSITIONS

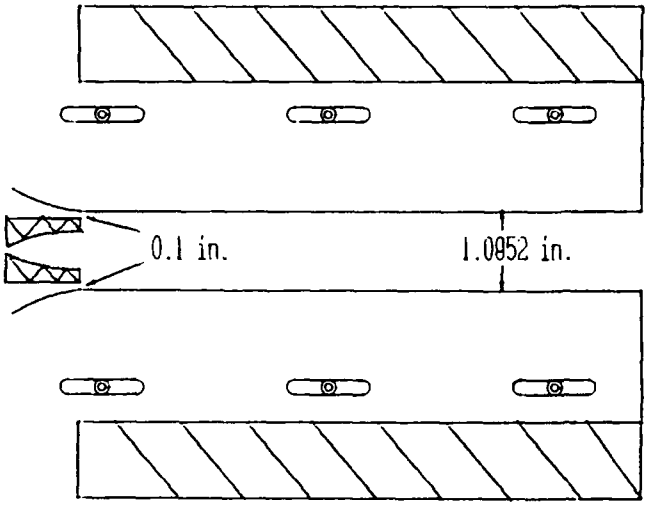

A. Small Secondary Throat and Mixing Chamber Cross-Section

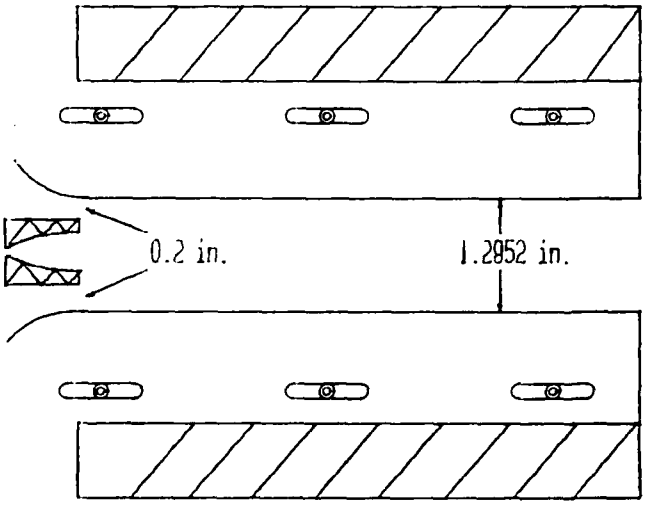

B. Large Secondary Throat and Mixing Chamber Cross-Section

FIGURE 7. VARIATIONS OF SECONDARY THROAT AND MIXING CHAMBER SIZE

mixing chamber so pressure transducers were only needed on one wall.

Finally, plexiglass windows extended from the nozzle throat to the end of the mixing chamber to allow for schlieren photography of the wave interaction.

Rocket Nozzle

One rocket nozzle and two different mixing chamber assemblies were used to provide the two-dimensional configurations studied. The rocket nozzle was designed using the method of characteristics as shown by Shapiro (5:462-528). Its throat dimension of 0.113 inch and exit dimension of 0.520 inch produced an area ratio of 4.6 which corresponds to an isentropic exit Mach of 3.09.

Instrumentation

Nine pressure transducers located as shown in Figures 8 and 9 were used to measure the data for all configurations and experiments. The wall pressures along the mixing chamber block were measured by six Endevco 8506-B transducers with a range of 0-5 psig. As mentioned previously, symmetry was assumed top and bottom within the mixing chamber as determined from schlieren photographs. These transducers were designated numbers P2, P3, P4, P5, P6, and P7. To measure absolute pressure, a near absolute vacuum was established on the rear face of each transducer diaphragm through a tube vent. This pressure became a

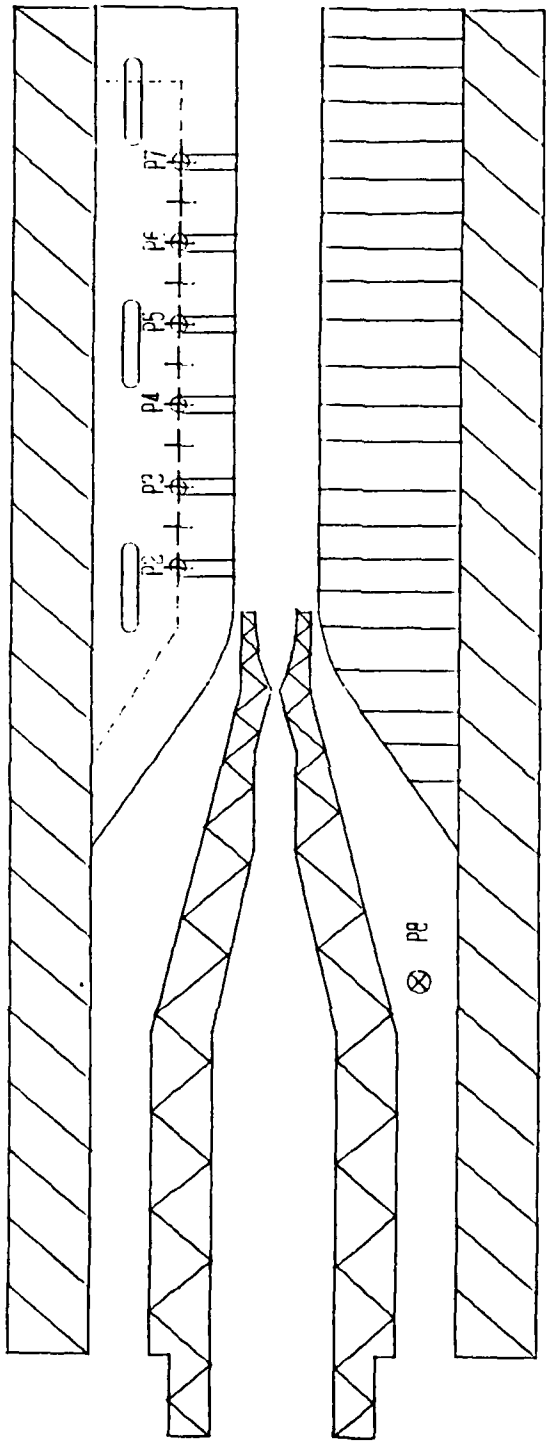

Figure 8. Test Section Transducer Location

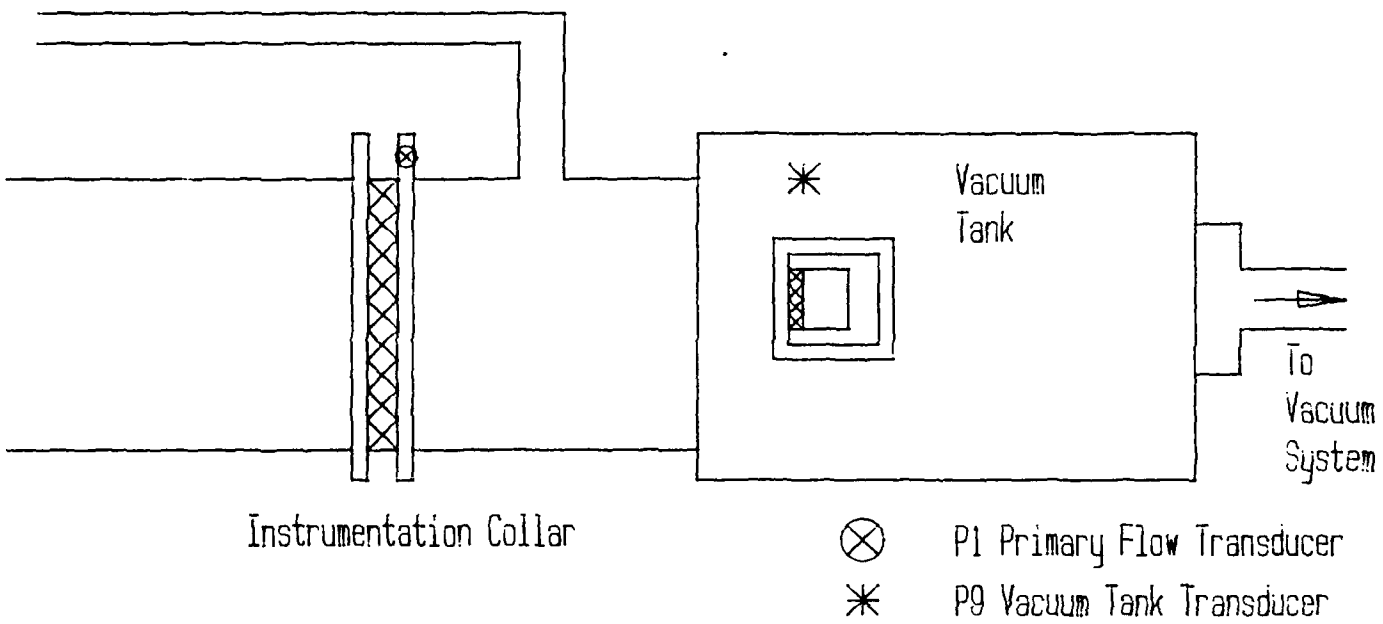

Figure 9. Flow System Transducer Location

reference to which the pressure acting on the external side of each diaphragm was compared.

Transducers designated P1 and P8 were Endevco 8530A-100 with a 0-100 psia range. P1 measured the upstream rocket nozzle plenum pressure (chamber stagnation pressure) and P8 measured the upstream ejector secondary flow plenum pressure.

One last transducer, P9, was placed on the vacuum tank. This transducer, an Endevco 8510-B with a 0-5 psig range, was used to measure the ambient pressure rise during the "descent" of the rocket. It was connected to the vacuum reference as were the 8506-B transducers. Table 1 shows the transducers by number, type, location, and serial number.

In support of the transducers, several other measuring devices were used. First, a mercury manometer was connected to the vacuum chamber to determine the vacuum in the tank prior to each run. Second, a Wallace and Tiernan precision gauge, model FA160 (S/N EE14201), was attached to the reference vacuum pump to ensure the near absolute vacuum was attained and maintained as a reference for the pressure transducers. Also, a Type CEC 2500 digital barometer was used to determine actual barometric pressure in the room during the experiment.

Schlieren System

In support of the objectives of this study, an investigation was made of the wave interactions throughout the mixing chamber under the various ejector operating

Table 1. Pressure Transducers

Location	Model Number	Serial Number
Rocket Plenum (P1)	Endevco 8530	44AM
Mixing Chamber (P2)	Endevco 8506	82BF
Mixing Chamber (P3)	Endevco 8506	83BF
Mixing Chamber (P4)	Endevco 8506	97BF
Mixing Chamber (P5)	Endevco 8506	74BF
Mixing Chamber (P6)	Endevco 8506	79BF
Mixing Chamber (P7)	Endevco 8506	68BF
Ejector Plenum (P8)	Endevco 8530	WL44
Vacuum Tank (P9)	Endevco 8510	PP79

conditions. The schlieren system shown schematically in Figure 10 was used to take still and video pictures of these phenomena. Black and white still photographs were taken using a spark lamp with a spark duration of less than one microsecond. Polaroid sheet film types 52 and 57 were used for the stills. Video pictures were taken using a Newvision video cassette recorder camera and a Kodak VHS tape.

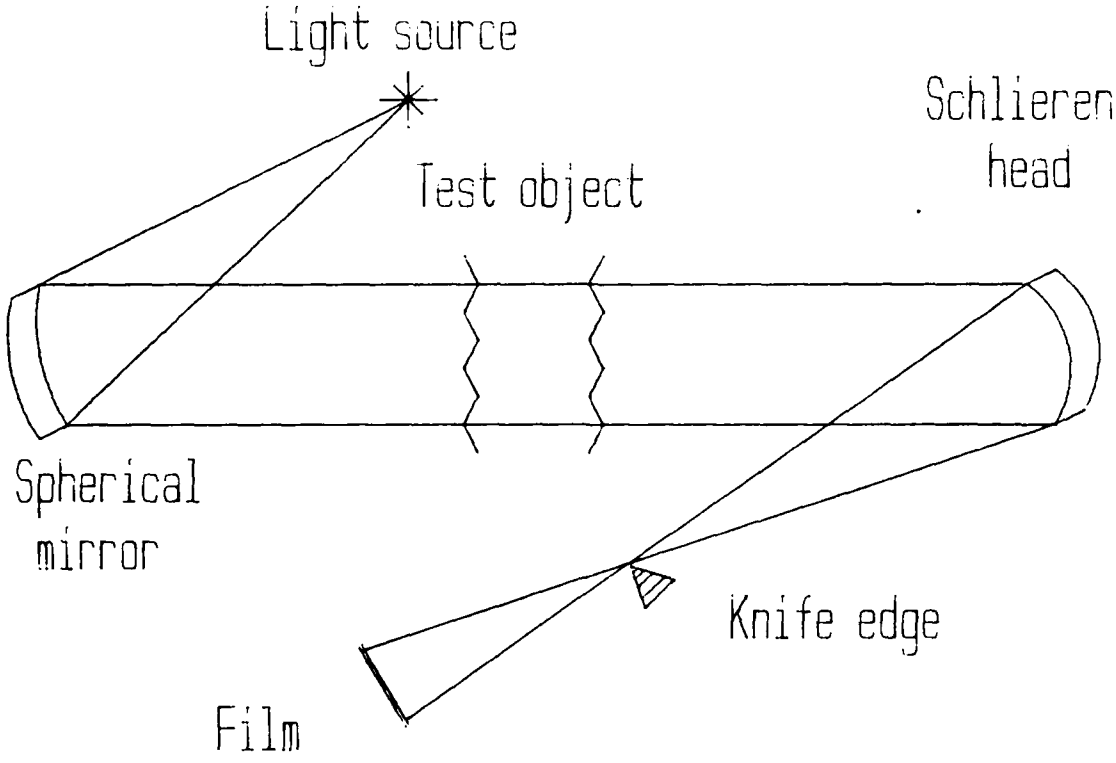

Figure 10. Schlieren System

IV. Data Acquisition and Reduction System

The Hewlett Packard (HP) 6901S Measurement and Analysis System is an automated digital system specifically selected for its enormous data collection capabilities. The experimental apparatus was designed to interface with the HP 6901S using the hardware listed in Table 2. The components were linked using the HP-IB interface bus as shown in Figure 11. The HP-IB serves as the centralized coordination center for several external devices such as the printer, plotter, and disk drive. The bus, which selectively controls data selection and flow rate to and from the peripheral devices, is controlled by the HP 9826 computer keyboard using a function select menu.

The HP 6901S is a multi-channel data acquisition and reduction system. It can collect data on up to 264 channels of either analog or digital data with a total collection capability of 4,096 samples per experiment. There are 16 interface cards available which can accommodate a sampling rate of 100,000 scans per second. This investigation required only a small portion of this capability. Figure 12 shows how the HP 6901S interfaces with the hardware.

The HP 6901S has an internally mounted HP 6942 multi-programmer. The HP 6942 contains the memory cards, analog to digital converters, scanner relays, and controller cards required for system operation. Data is acquired through the HP 6901S terminal boards and is temporarily stored so the

Table 2. Instrumentation Hardware

Item	Model Number	Serial Number
Power Supply	HP 6205C	2208A-00631
Multiprogrammer	HP 6942A	2513A-06003
Computer	HP 9826	2313A-05860
Plotter	HP 7470A	97468
Printer	HP 2934A	2635A-32528
Measurement and Analysis System	HP 6901S	234A-00104
Portable Vacuum Standard	PVS-2A-10000	44362-1

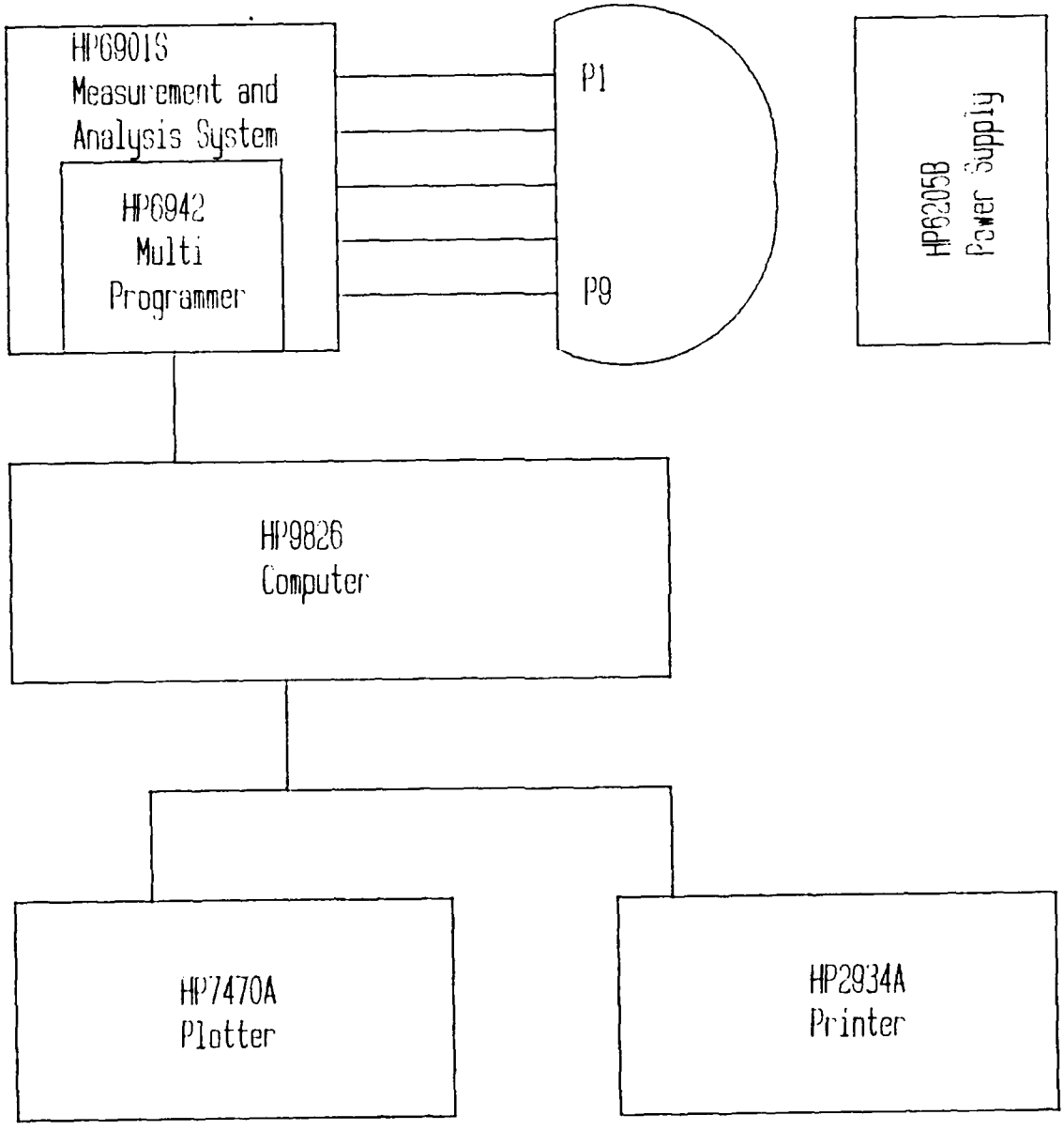

FIGURE 11. HARDWARE COMPONENTS

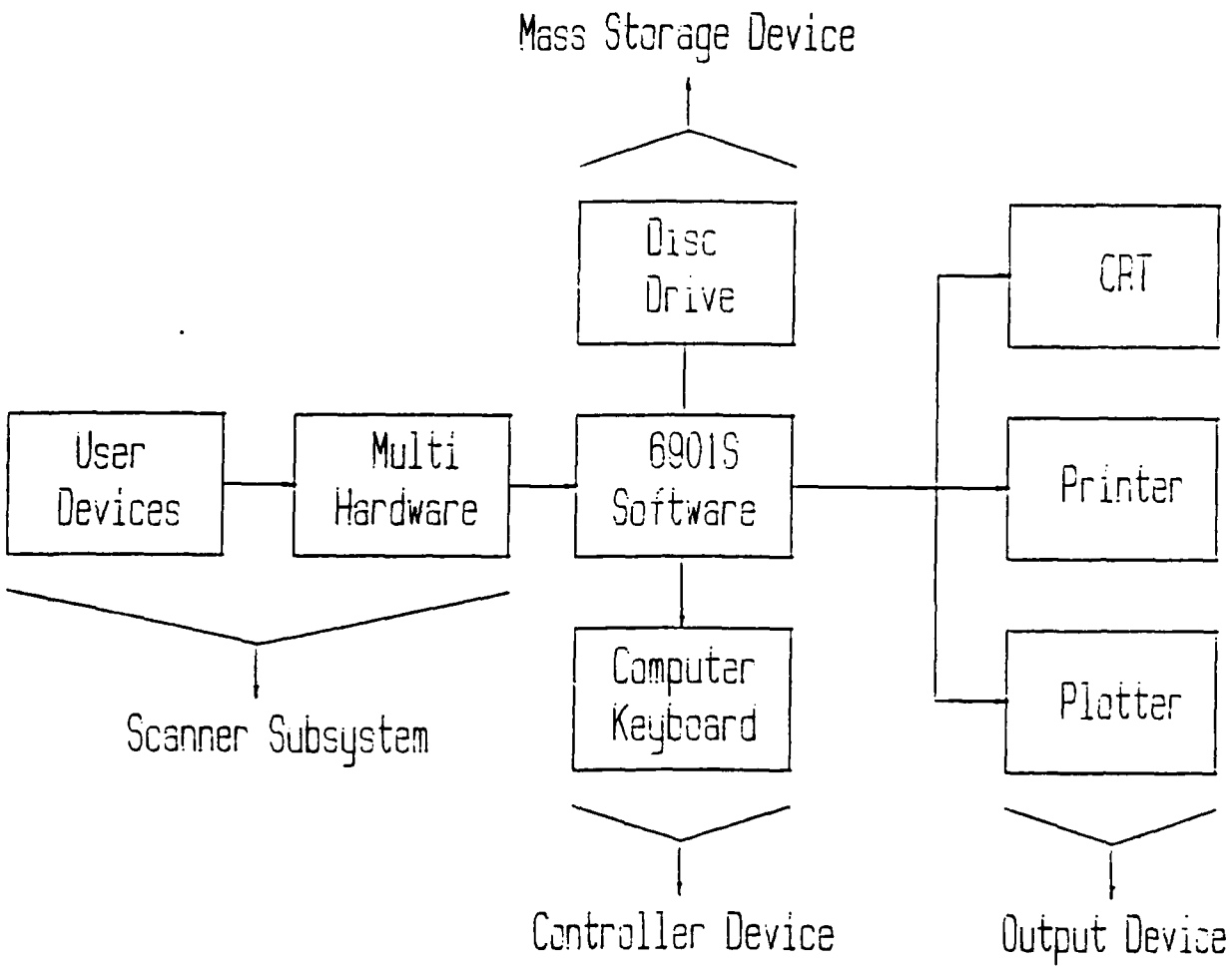

Figure 12. HP6901S System Schematic

desired sampling rate can be achieved without exceeding the capacity of the analog to digital converter. The data is recalled sequentially from storage, converted to digital form and sent to the HP 9826 for storage on floppy disk. This sequence is shown in Figure 13.

The HP 9826 computer shown in Figure 11 is a menu driven system controlled from the keyboard. The menu options (see Figure 14) provide the means for entering the experimental apparatus parameters. These parameters, including scan rate, number of scans, and the data acquisition initiation or triggering mode, were entered using the HP 6901S software. Data was collected using the burst mode option. The high speed scanning capability of this mode allowed nearly simultaneous monitoring of all channels. Run time for this experiment ranged from two to four minutes depending on the amount of secondary flow being used. Therefore, the system was set to scan all nine channels every 0.3969 seconds. This rate provides 58,800 microseconds between scans of each individual channel for a total of 455 scans. Since this study was more concerned with the pressure from sea level to 50,000 feet, the scan rate needed to be increased from that used in previous theses to ensure data was taken over the entire altitude range.

Several data presentation options were available. However, of the tables, graphs, or histograms, a multi-

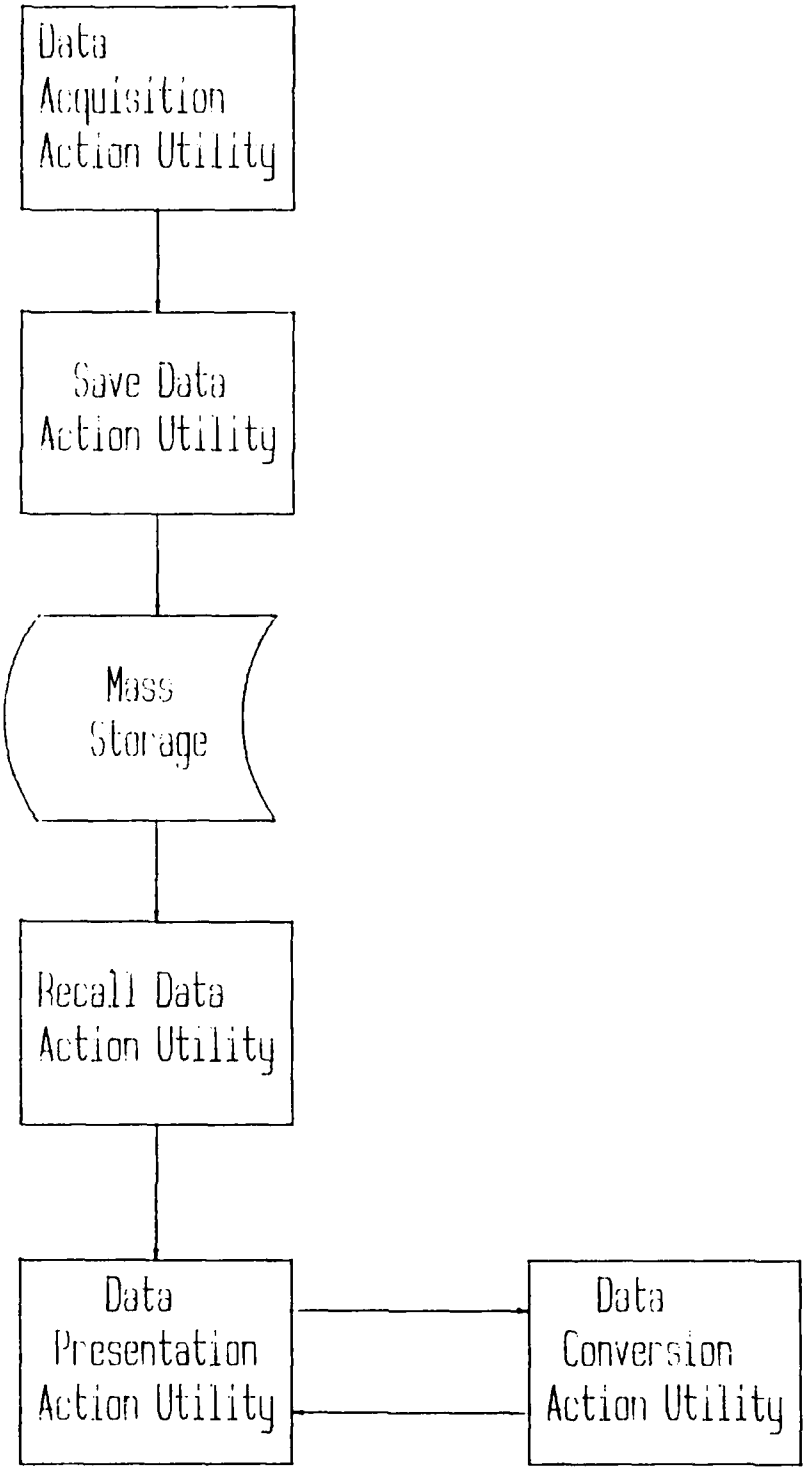

Figure 13. Data Flow Path

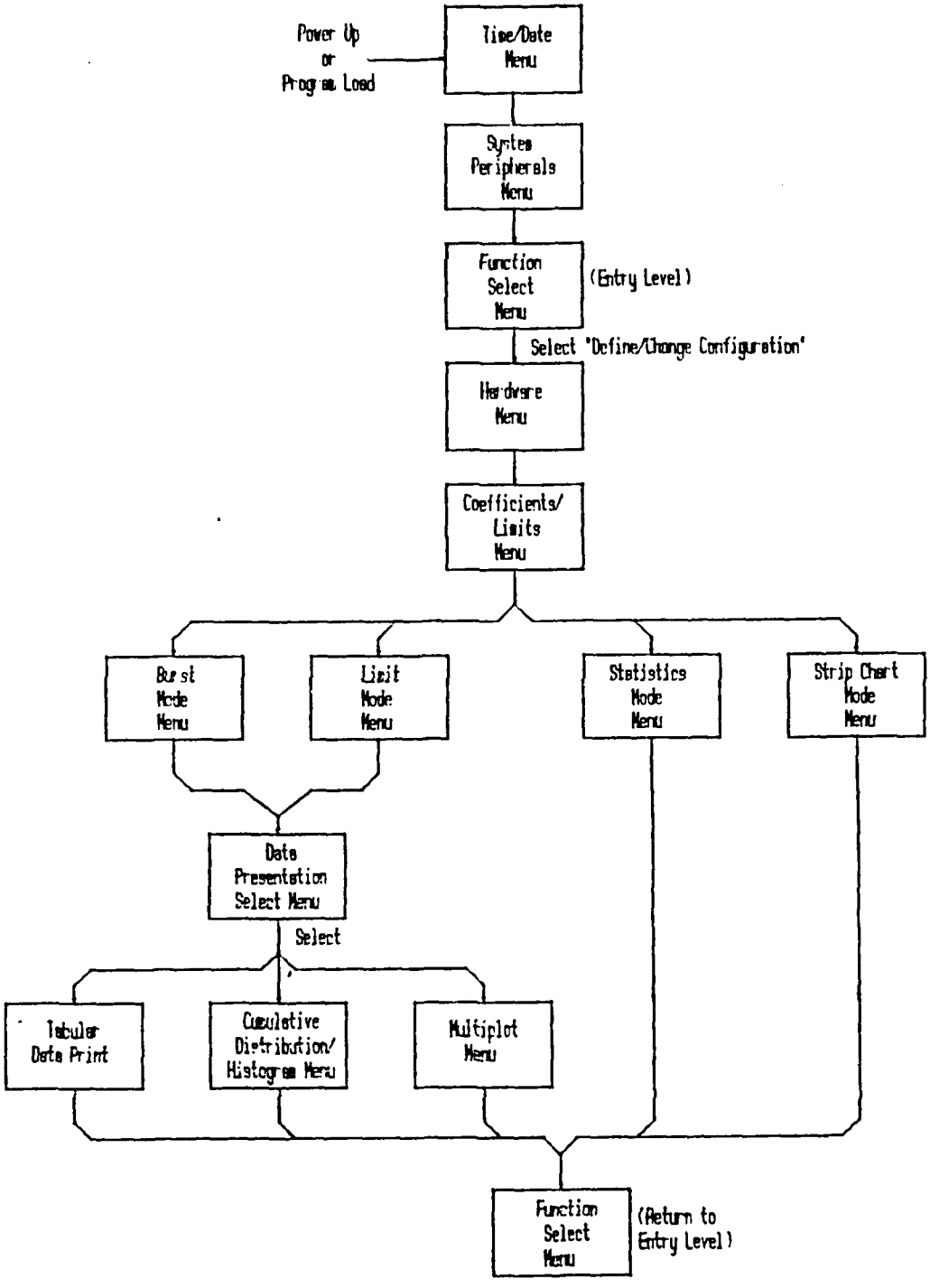

FIGURE 14. FUNCTION SELECT MENU

channel plot option was primarily used. This option displayed up to eight channels at one time. A key option allowed for windowing and zooming in on the data for a more detailed view. Having nine channels was only a minor drawback since any more than two channels displayed simultaneously was somewhat difficult to interpret. Data reduction, including inserted offset values used to scale the data, was accomplished prior to receiving the selected output presentation.

This system was suitable for the research done on the blowdown wind tunnel. The pressure characteristics along the wall and in the tunnel were adequately acquired, processed, and formatted. The system is easily expandable for future study.

V. Experimental Procedure

As in all experimental work, continuous checking of equipment is required to ensure proper output. This begins with the initial calibration of the equipment to ensure proper interpretation of collected data. It also includes daily equipment checks to avoid possible changes in conditions over the course of experimentation. Finally, actual data collection must be followed by close scrutiny of collection procedures to be absolutely certain of consistent results.

Calibration

All of the transducers were calibrated using a dead weight pressure system. This system provided a reference pressure on one side of the measurement diaphragm which compared with air pressure from a separate source acting on the other side of the diaphragm. The pressure differential produced a voltage differential. The weights were added in small increments to increase the pressure throughout the range of the transducers. The voltage generated from this pressure difference was recorded on a digital voltmeter, plotted on a graph, and used to produce a slope which represented the transducer sensitivity in millivolts per psi. The sensitivity was linear over the full range of the transducers and was always within 3% of the manufacturer's calibration.

Experimental Run Procedure

Since consistent data collection is a primary goal in all experimental work, each experimental run should be made using the same procedure. This was done for this study. To establish the desired initial test conditions, the three primary vacuum pumps were turned on to evacuate the chamber. An excitation voltage of 10 volts D.C. was applied to the transducers and the reference vacuum pump for the transducers was turned on. The approximate reference pressure of 1 mm Hg was established.

The computer was then turned on and the SHELL software program of the HP 6901S Measurement and Analysis System was loaded and run. The time and date were entered on initial power up to ensure adequate tracking of data. Once the proper "Configuration File" was selected based on the data required, the program's "Run Current Configuration" option was selected from the Function Select Menu shown in Figure 14. The current configuration file established the proper transducer scaling information necessary to reduce the pressure data for presentation. The configuration also provides for a data collection start procedure. An external trigger was used to allow manual starting of data collection. The multichannel plot option was selected which provided for eight of the nine transducers to plot pressure versus time on a single hard copy graph.

After selecting "Run Current Configuration," a four-second self test is accomplished by the system to ensure all

integrated circuit cards are properly placed so that no major hardware failures will occur. At this point, a data file is created and the program awaits the triggering system to begin collecting data.

Once the vacuum tank pressure reaches approximately 0.1 psia, the pressure transducers are balanced or "zeroed-out" by adjusting the potentiometer to ensure identical input and output voltage on the HP6901S system. The balancing circuitry includes a differential amplifier with a gain of one between the potentiometer and the input voltage to reduce background noise. Figure 15 shows a schematic of the potentiometer amplifier circuit which converts the output from two-wire to one-wire to be suitable for the HP6901S.

The experiment could now be performed. Data acquisition system operation was initiated and the main hand-operated disk-valve was opened allowing the flow into the test section. During the run, the lights were turned off and schlieren photographs were taken at pre-determined time intervals. These photographs would be correlated with the data taken to help visualize the flow conditions in the mixing region and how they change with increase of back pressure.

After the run time elapsed, the hand valve was closed. The HP 9826 computer stored the data and produced it for hard copy form. Each run was duplicated to ensure conformity of data collection.

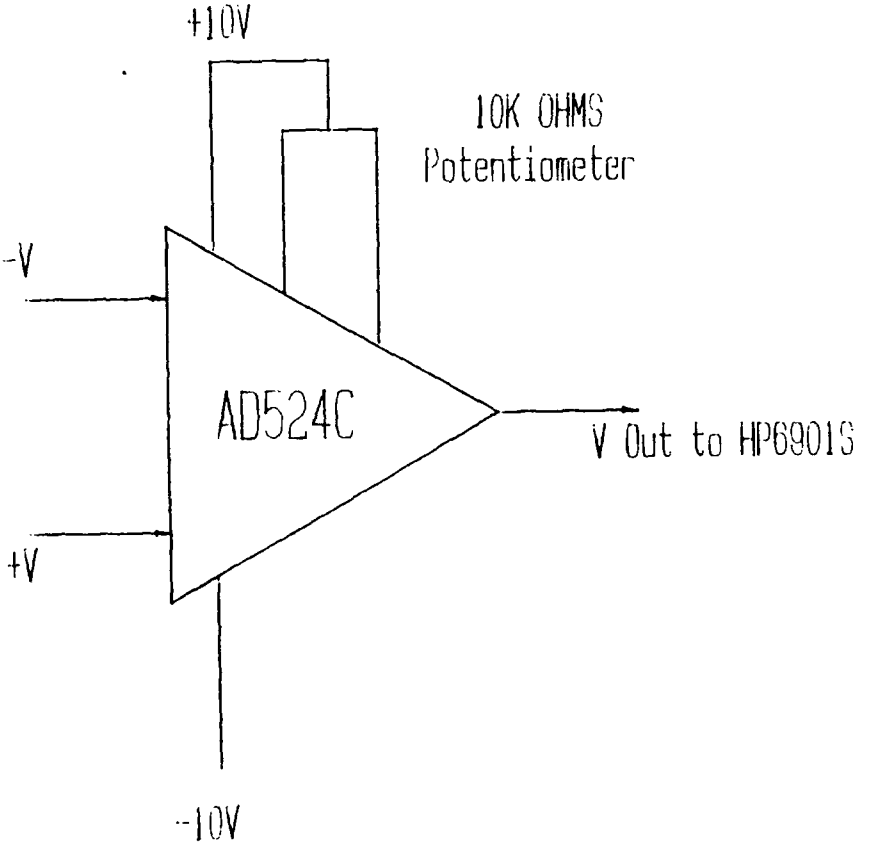

Figure 15. Potentiometer Amplifier

During each run, the primary rocket nozzle was supplied a plenum pressure of approximately 110 psia. The ejector secondary flow was supplied air from a separately regulated plenum. This flow was adjusted to simulate conditions ranging from static launch with sea level pressure to a ram generated flow representing vehicle velocity changes.

Data Explanation

Each run used to generate the selected launch profile produced a series of pressure measurements for each of the transducers over the entire run period. This data was used to provide several useful foundations for data comparisons.

The vacuum tank pressure, P9, was used to transform the time information provided by the HP6901S measurement system into altitude. By using equations representative of the ARDC standard atmospheric tables (14), the resulting altitude data became the basis for comparison of other pressure information. Appendix A contains this procedure.

The simulated vehicle Mach number was deduced using the secondary plenum pressure, P8, and the vacuum tank pressure, P9. The Mach number was calculated with the isentropic relationship

$$\frac{P_T}{P} = \left(1 + \frac{k-1}{2} M^2\right)^{(k/k-1)} \qquad (4)$$

where

P_T = ejector secondary flow total pressure (psia)

P = vacuum tank ambient static pressure (psia)

k = specific heat ratio

= 1.4 for air

M = Mach number

The calculated values of Mach number and altitude can be plotted together to reflect a flight profile on each run. A typical output is represented by Figure 16. While a wide variety of profiles were produced, one individual run does not simulate the actual effect of a static launch followed by a ram-induced increase in velocity because for each run the secondary pressure was held constant. The shuttle profile presented in Figure 1 will be used as a basis to select the experimental data from various runs to closely simulate this profile.

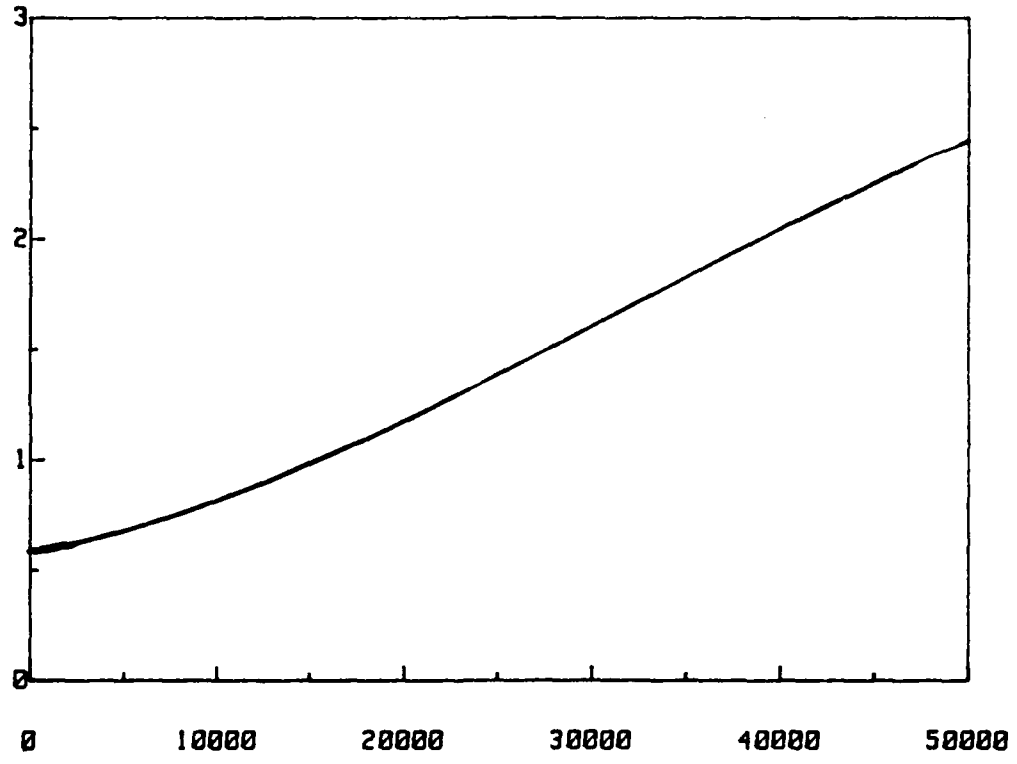

FIGURE 16. TYPICAL MACH NUMBER VS ALTITUDE PLOT

VI. Results and Discussion

The AFIT blowdown wind tunnel was used to simulate the environment an ejector-rocket would encounter during a launch. While a normal rocket would proceed from a sea level launch into the low pressure environ of high altitude, the blowdown facility reverses this profile by starting in a near vacuum and continually increasing back pressure or decreasing altitude. Therefore, where a rocket would normally transition from the overexpanded flight regime through the design point of the nozzle to the underexpanded regime, this experiment proceeds in the opposite direction.

General Experimental Run Comparisons

Before the data is selected to represent the selected launch profile, a general explanation of the separate runs is addressed. Two sets of mixing chamber walls were used which allowed variation in secondary throat size and relative position of the primary nozzle. The comparisons are made based on three areas:

1) Secondary flow pressure comparisons

2) Throat position comparisons

3) Mixing chamber assembly comparisons

Secondary Flow Pressure Comparisons. The secondary flow was adjusted by the Grove regulator and the use of the atmospheric pressure control valve to provide the Mach number and altitude scenario for a particular test run. The

effect of increasing the secondary total pressure from ambient pressure up to 35 psia may be observed from equation 4. Since the static pressure will rise as the flow enters the vacuum tank similarly for each test, the ratio of P_T/P will obviously be larger with increasing secondary total pressure. The result is a larger simulated Mach number at a given altitude as P_T increases. The effects of the larger total pressures, representative of reaching higher Mach numbers at lower altitudes during a launch can be seen from Figure 17. While the wall pressures near the exit plane of the nozzle and ejectors remain relatively small and constant regardless of secondary total pressure at the higher altitudes (greater than 30,000 feet), the effects are varied at the lower altitudes but do have some trends.

Schlieren pictures (video and stills) and raw data suggest the wall pressures exhibit a transition point which is a reflection of the combined effects of the increasing back pressure and secondary total pressure. Figure 18 gives a visual presentation of the effect the back pressure increase has on the chamber flow. While the video clearly showed the fluctuations actually occurring within the mixing chamber, the still pictures reflect the difference between the obviously unaffected area near the nozzle and ejector exits at higher altitudes (Figure 18A) and the back pressure affected area downstream as altitude decreases (Figures 18B and 18C). The increased secondary pressure provides a larger mass flow rate into the vacuum tank which causes its

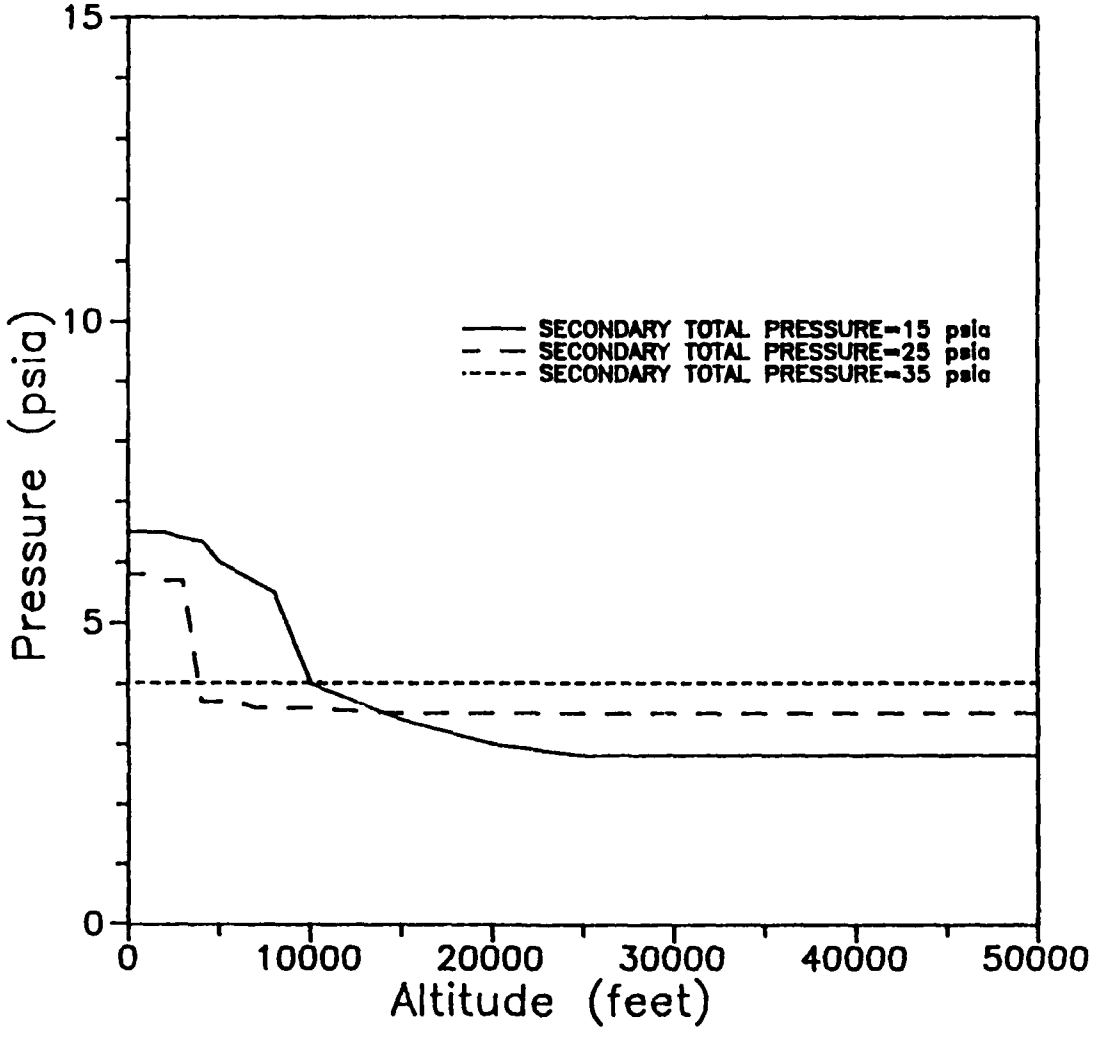

FIGURE 17. WALL PRESSURE P3 VS ALTITUDE INCREASING SECONDARY TOTAL PRESSURE

A. LOW BACK PRESSURE

B. INCREASING BACK PRESSURE

C. SEA LEVEL CONDITIONS

FIGURE 18. BACK PRESSURE EFFECTS ON MIXING CHAMBER FLOW

pressure to increase faster. The resulting effect from this is the movement of the highly turbulent section of air due to the separation of the shocks from the walls at earlier times which means higher altitudes. Figure 19 shows the transition points (back pressure induced pressure rises) at transducer P5 of two separate runs, a low secondary pressure of 15 psia and a high pressure of 27 psia. While it appears that the transition points are fairly close (50 seconds for Figure A and 60 seconds for Figure B), these translate into a 12,000 feet altitude difference (see Figure 20).

Keeping in mind the reverse trajectory simulated in the chamber, a major point that can be seen is the higher, more fluctuating pressures which occur at the lower altitudes would last longer if the profile is selected which reaches higher Mach numbers sooner. While the high wall pressures could mean more pressure thrust increases, the large fluctuations could provide structural problems that may need to be considered.

Throat Position Comparisons. The relative throat position of the primary nozzle and the mixing chamber was adjusted by sliding the mixing chamber wall assembly forward or aft on channels cut out of the plexiglass. The positioning of the walls not only affected the position of secondary flow throat but its size as well.

The primary effect of adjusting the position of the secondary flow throat for this model is very evident by looking at the photographs in Figure 21. Photograph A shows

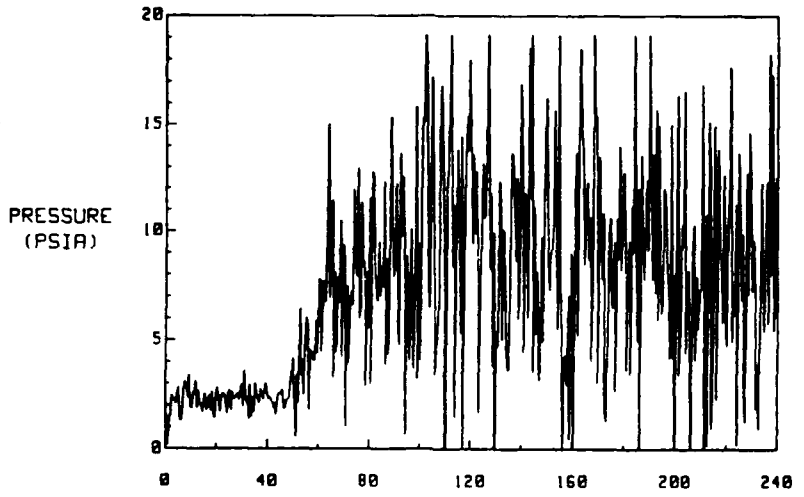

A. WALL PRESSURE P5 TRANSITION FOR 15 PSIA SECONDARY PRESSURE

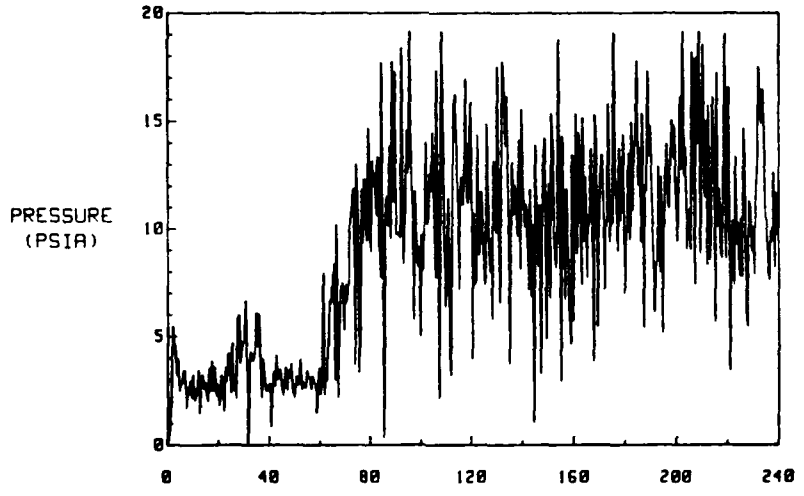

B. WALL PRESSURE P5 TRANSITION FOR 27 PSIA SECONDARY PRESSURE

FIGURE 19. WALL PRESSURE P5 TRANSITION
FOR 15 PSIA AND 27 PSIA SECONDARY TOTAL PRESSURE

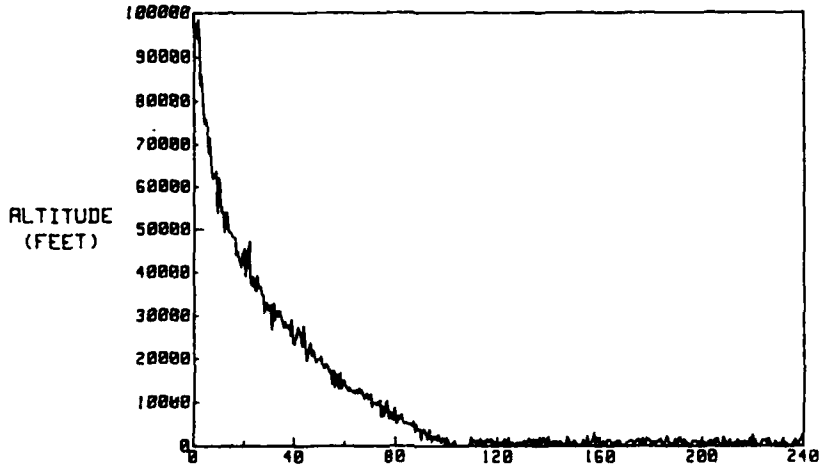

A. ALTITUDE VS TIME FOR 15 PSIA SECONDARY PRESSURE

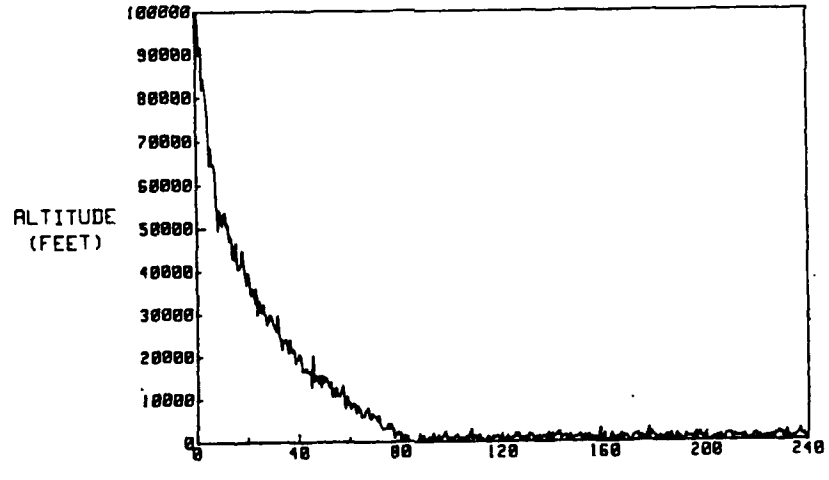

B. ALTITUDE VS TIME FOR 27 PSIA SECONDARY PRESSURE

FIGURE 20. ALTITUDE VS TIME
FOR 15 PSIA AND 27 PSIA SECONDARY TOTAL PRESSURE

A. PRIMARY AND SECONDARY EXIT PLANES CO-LOCATED

B. PRIMARY NOZZLE 1/2 INCH INTO MIXING CHAMBER

C. PRIMARY NOZZLE 1/2 INCH FORWARD OF MIXING CHAMBER

FIGURE 21. FLOW COMPARISONS WITH THROAT VARIATIONS

the flow with the secondary flow throat co-located with the primary nozzle exit plane. Photograph B shows the flow with the walls adjusted so the primary nozzle exit plane is actually moved 1/2 inch into the mixing chamber. There is relatively little difference in the shock pattern between photographs A and B. Photograph C shows the walls have been adjusted to move the primary nozzle forward of the mixing chamber. From the photograph as well as referring back to Figure 6, it is evident that the secondary flow is angled into the chamber rather than flowing in axially as the primary flow does in all cases and the secondary flow does in the other two cases.

While the overall effect of this angularity is unknown and will require further study, it is evident that the wall pressures nearest to the nozzle exit plane are most affected. Figure 22A shows the plot for the wall pressure one inch from the exit plane of the nozzle with the nozzle plane 1/2 inch into the chamber. Note the relatively constant pressure of approximately 3 psia which is the expected pressure exiting the nozzle at Mach 3.09. The transition occurs at 90 seconds for which the ambient back pressure corresponds to approximately 5,000 feet. The resulting wall pressure fluctuates around an average of 6 psia. In Figure 22B, while the wall pressure is highly oscillatory, it remains relatively constant at an average of 8 psia at the same mixing chamber location.

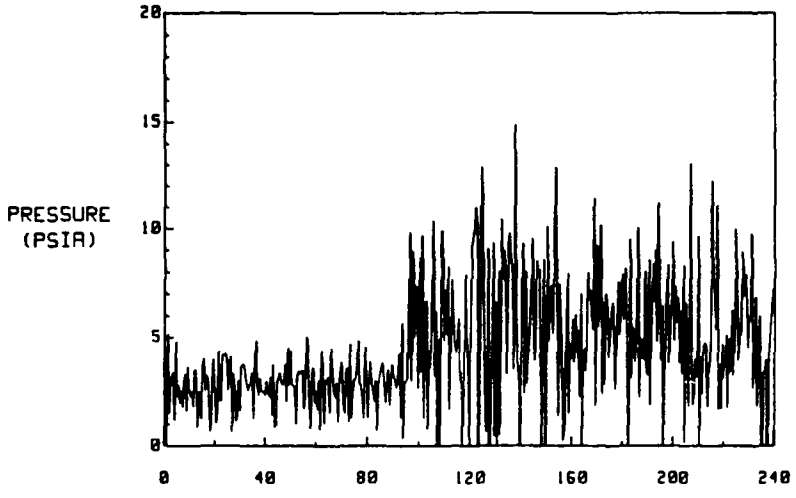

A. WALL PRESSURE P3 FOR NOZZLE INTO CHAMBER POSITION

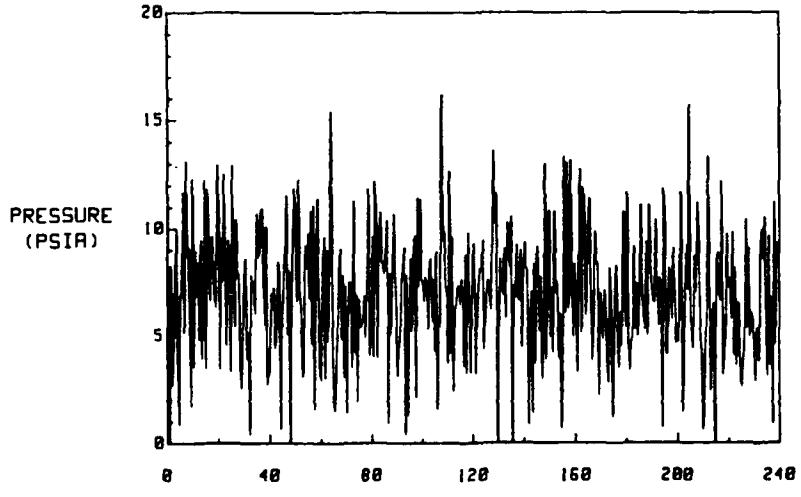

B. WALL PRESSURE P2 FOR NOZZLE FORWARD OF CHAMBER POSITION

FIGURE 22. WALL PRESSURE COMPARISONS FOR NOZZLE INTO AND NOZZLE FORWARD OF MIXING CHAMBER

Figure 23 shows the schlieren photographs for these two runs. The first two reflect the different stages represented by the data in Figure 21A. The transition effects are visually evident from these pictures. The next two photographs show flow characteristics for the nozzle exit plane ahead of the mixing chamber at the same time and altitude points as the first run.

The flow as shown in Figure 23A is primarily axial entering the mixing chamber and there is a very obvious shock pattern formed which affects the pressure at the transducer one inch from the exit plane at the higher altitudes. As the altitude decreases, the ambient back pressure increase causes the flow to detach from the chamber walls and the secondary flow is drawn into the center. The transducer output changed as a result of this change of flow conditions and shock pattern.

Figure 23C shows an angular secondary flow entering the ejector mixing region at high altitude. The result of this is a region near the ejector mixer entrance which apparently is not affected by altitude changes. Accordingly, the flow is not affected, nor is the wall pressure at this location.

Mixing Chamber Assembly Comparisons. Two mixing chamber assemblies were used during this experiment. The primary purpose was to study the effects of varying secondary mass flow on the wall pressures and flow phenomena. The difference between the chambers was an increase in the chamber area from 1.095 to 1.295 square

A. NOZZLE INTO MIXING CHAMBER, HIGH ALTITUDE

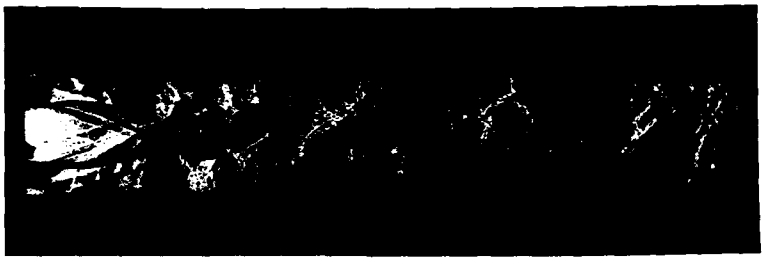

B. NOZZLE INTO MIXING CHAMBER, SEA LEVEL

C. NOZZLE FORWARD OF MIXING CHAMBER, HIGH ALTITUDE

D. NOZZLE FORWARD OF MIXING CHAMBER, SEA LEVEL

FIGURE 23. TRANSITION EFFECTS WITH THROAT VARIATIONS

inches while increasing the ejector secondary flow throat from 0.1 inch to 0.2 inch. Recalling the formula

$$m = \frac{MFP\ P_T\ A}{(T_T)^{1/2}} \qquad (5)$$

where

m = mass flow rate (lbm/sec)

MFP = mass flow parameter ($lbm\text{-}(°R)^{1/2}/lbf\text{-}sec$)

P_T = total pressure (psia)

A = cross-sectional area (in^2)

T_T = total temperature (°R)

it is obvious that with everything else held constant, doubling the area at throat of the ejector secondary flow will double the mass flow rate.

The immediate effect of this change in the physical experiment is the more rapid rise of the vacuum tank pressure due to the large mass flow of air being discharged into it. The effect seen within the simulated environment is a much faster "descent" from altitude. These effects are translated to the data with two relatively common results.

Figure 24 shows a comparison of similar runs which only have a difference in mixing chamber and ejector secondary flow throat size. The wall pressure P6, near the rear of the chamber, is shown in each figure. Figure 24A has the smaller throat and mixing chamber but does not see any appreciable difference in initial wall pressures (at the higher altitudes) or the resulting pressures after

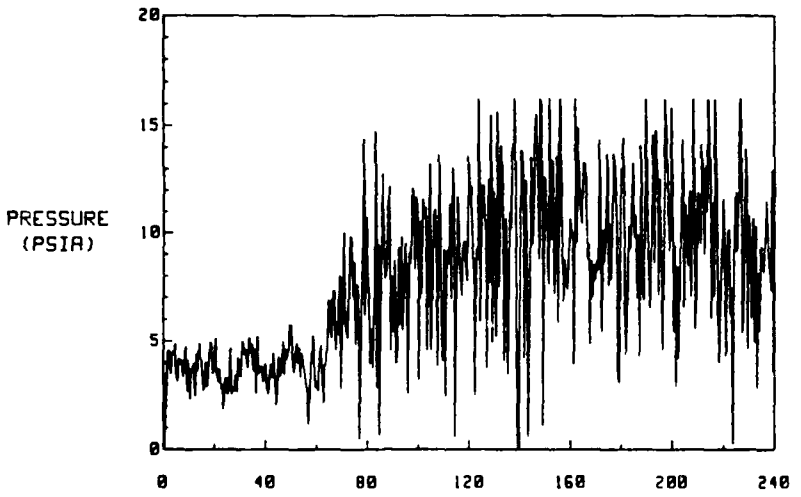

A. WALL PRESSURE P6 FOR SMALL CROSS-SECTION THROAT AND CHAMBER

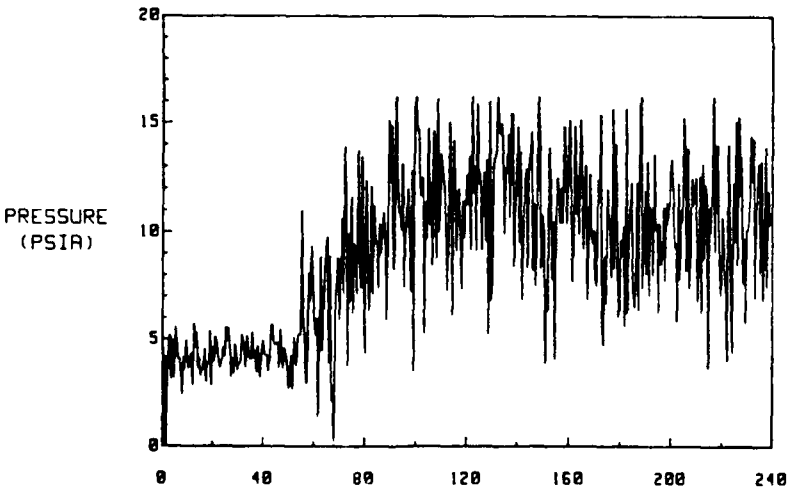

B. WALL PRESSURE P6 FOR LARGE CROSS-SECTION THROAT AND CHAMBER

FIGURE 24. WALL PRESSURE P6 FOR SMALL AND LARGE CROSS-SECTIONS

transition compared with Figure 24B with the larger secondary throat. Note that while Figure 24A shows a transition at 65 seconds and Figure 24B shows a transition at 55 seconds, the altitude versus time curves for these two runs reveal these points to be about the same at 10,000 feet (see Figure 25).

In contrast for the same runs, wall pressure P3, near the nozzle exit plane, is shown in Figure 26. Two points must be considered. First, while the high altitude pressures are of similar fluctuation and value, the transition points for the two runs correspond to 5,000 feet for the smaller throat and chamber and over 15,000 feet for the larger. Also, the resulting wall pressure at the lower altitudes is much higher for the larger chamber.

Schlieren photographs for these runs are presented in Figures 27 and 28. The effects noted can be seen from these photographs. The similarity of the flows, particularly downstream in the chamber, reflects the data results of Figure 24. The differences can be seen near the nozzle and secondary flow exit planes where a somewhat different shock pattern is formed for the larger secondary throat. This shock pattern extends closer to the transducer location (one inch from the exit planes) and thus causes the high, more fluctuating pressures than the smaller ejector produces.

Selected Profile Comparisons

Since the experimental runs simulated a reverse flight profile and the data, pictures and video reflect this

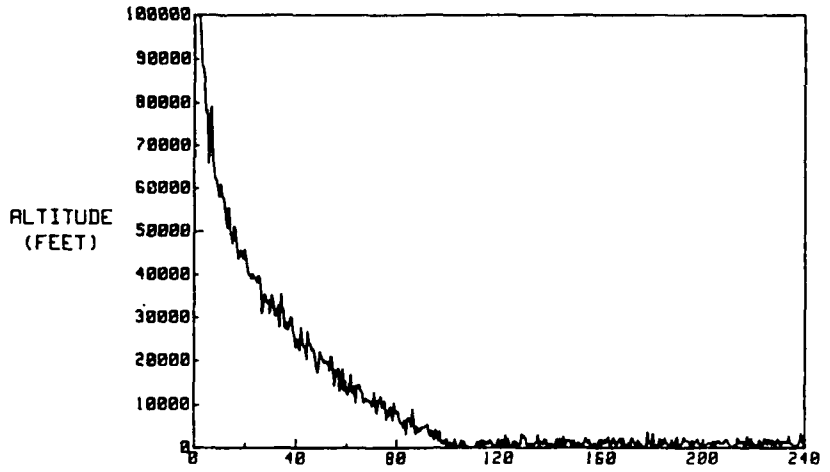

A. ALTITUDE VS TIME FOR SMALL CROSS-SECTION THROAT AND CHAMBER

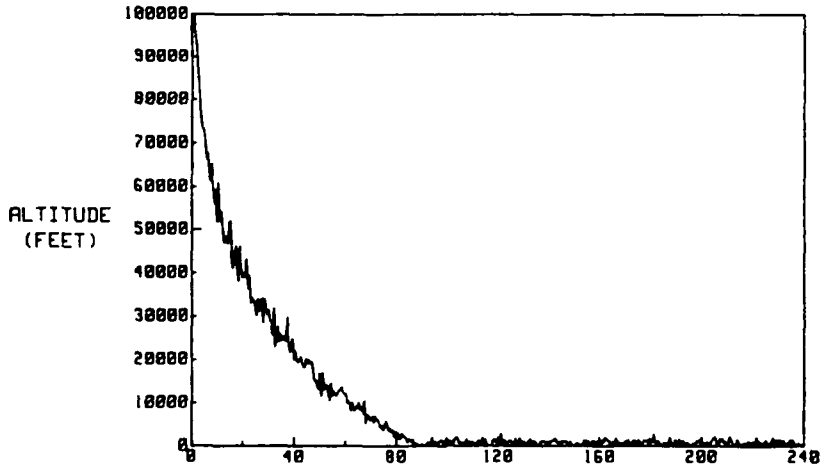

B. ALTITUDE VS TIME FOR LARGE CROSS-SECTION THROAT AND CHAMBER

FIGURE 25. ALTITUDE VS TIME FOR SMALL AND LARGE CROSS-SECTIONS

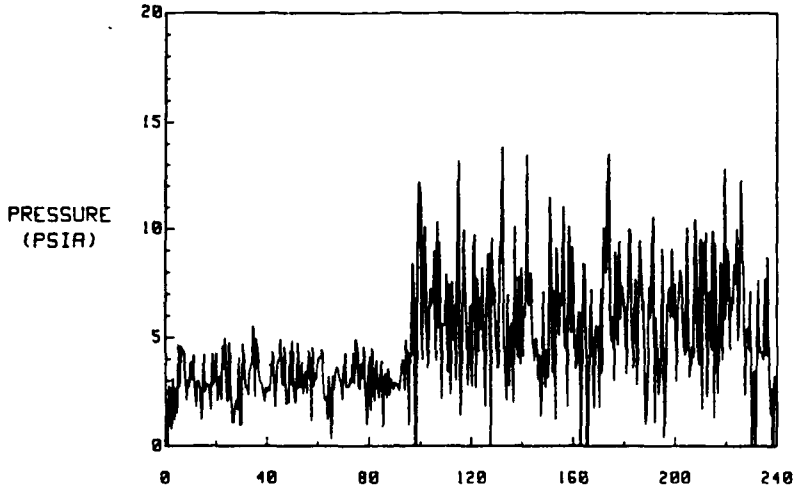

A. WALL PRESSURE P3 FOR SMALL CROSS-SECTION THROAT AND CHAMBER

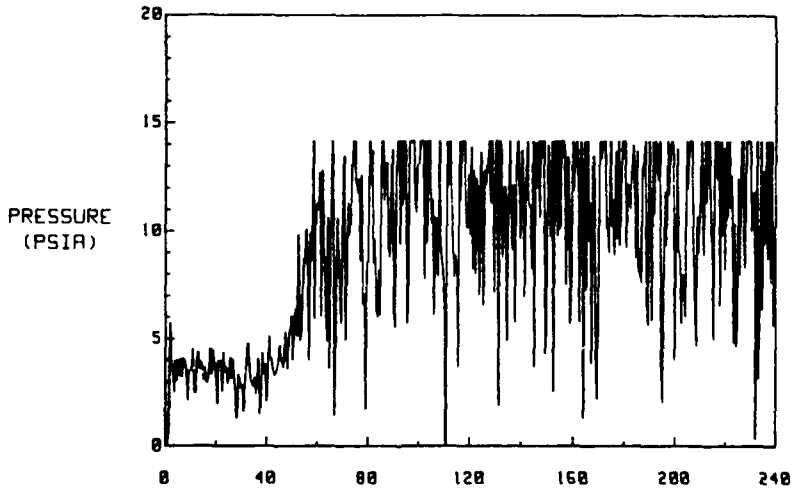

B. WALL PRESSURE P3 FOR LARGE CROSS-SECTION THROAT AND CHAMBER

FIGURE 26. WALL PRESSURE P3 FOR SMALL AND LARGE CROSS-SECTIONS

A. LOW BACK PRESSURE

B. INCREASING BACK PRESSURE

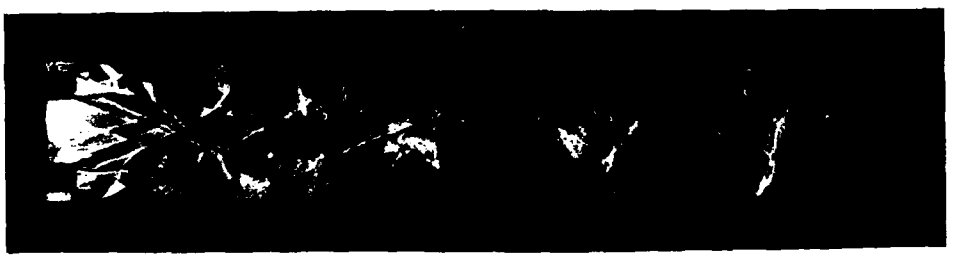

C. SEA LEVEL CONDITIONS

FIGURE 27. BACK PRESSURE EFFECTS ON SMALL CROSS-SECTIONS

A. LOW BACK PRESSURE

B. INCREASING BACK PRESSURE

C. SEA LEVEL CONDITIONS

FIGURE 28. BACK PRESSURE EFFECTS ON LARGE CROSS-SECTIONS

chronology, the discussion of the selected runs will proceed from the higher to the lower altitudes.

High Altitude Runs. The high altitudes are grouped together due to the unchanging results of the data. Figure 29A shows the schlieren photograph representative of all the runs used in simulating the higher altitude phase (30,000 feet and up) of the launch. During this phase, the shock pattern through the mixing chamber is well established. The strength of these shocks is relatively weak since the wall pressures remain fairly constant through the chamber. While the pressures remain constant, the back pressure continues to increase as the altitude decreases. The ratio of P_w/P_a decreases as altitude decreases (see Figure 30). While the results are not totally certain, if the last wall pressure, P7, closely represents the exit pressure of the system, P_e, this ratio decrease would indicate a reduction in the pressure thrust term from equation 1. This is not unexpected since most nozzles are designed to operate at higher altitudes. The magnitudes of the pressure thrust terms would need closer scrutiny to determine final advantages or disadvantages associated with the rocket nozzle-ejector system.

Transition and Low Altitude Runs. The transition that the wall pressures encounter during an individual experimental run is harder to distinguish in this composite study of several runs simulating one profile. While a definite rise in wall pressures does occur, the expected

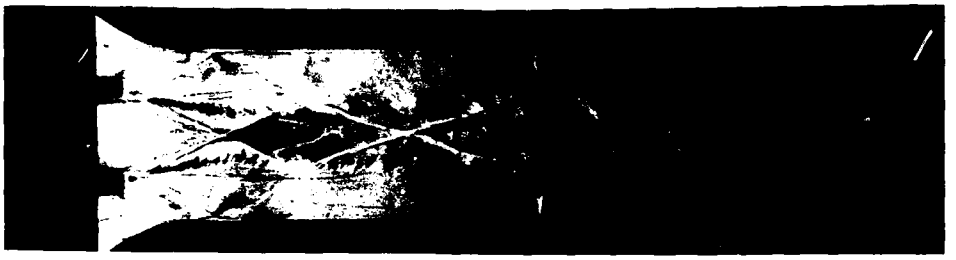

A. LOW BACK PRESSURE

B. INCREASING BACK PRESSURE

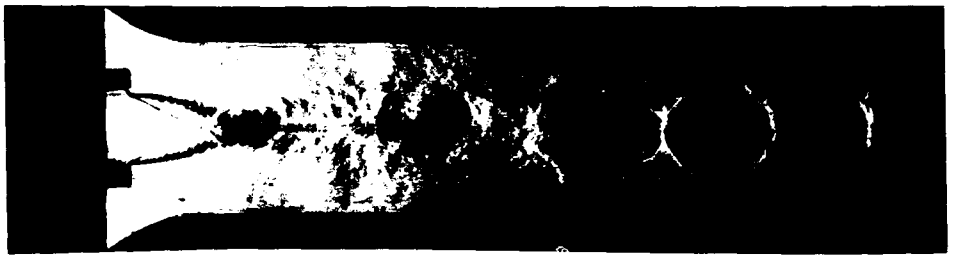

C. SEA LEVEL CONDITIONS

FIGURE 29. TYPICAL HIGH ALTITUDE RUN FOR SELECTED PROFILE

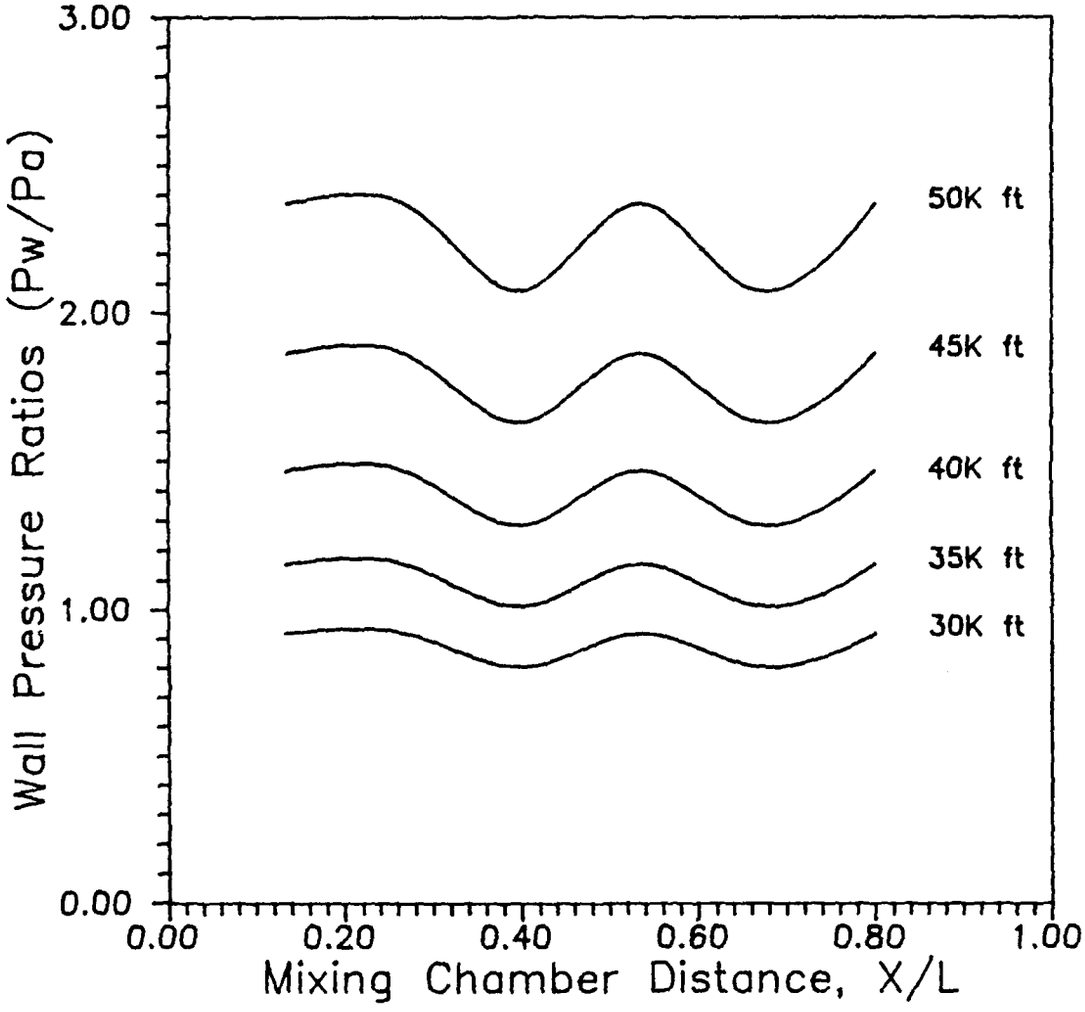

Figure 30. Wall Pressure Ratios for High Altitude

rise of the mixing chamber wall pressures which during the individual experimental runs began at the exit of the mixing chamber and propagated back toward the rocket nozzle and secondary flow exit planes does not occur. The rise encompasses the entire chamber at one time. This may more accurately describe what should happen since this selected change in altitude and Mach number does not occur in this order on any one run accomplished. One hypothesis for this pressure rise throughout the chamber at one time may be drawn from the photographs of Figure 31. At low altitudes when the flow transitions, it occurs rapidly and over the entire chamber (note in particular Figures 31B and C). Thus, when transition takes place, there is not any distinction between when the effects are noticed near the exit plane of the mixing chamber versus when the beginning of the chamber receives the same effect.

Figure 32 describes the wall pressure changes at the lower altitudes. While it is a very busy plot, several points need to be discussed. Note that some of the pressures start at X/L of 0 and some start at 0.13333. Since some of the selected runs were made with the nozzle in the aft position and some with the nozzle in the forward position, the transducers were at different locations relative to the nozzle exit plane and this difference is reflected on the graph by a shift of abscissa for beginning and ending the curves. One very evident point which reflects that transition has already occurred is the

A. LOW BACK PRESSURE

B. INCREASING BACK PRESSURE

C. SEA LEVEL CONDITIONS

FIGURE 31. TYPICAL LOW ALTITUDE RUN FOR SELECTED PROFILE

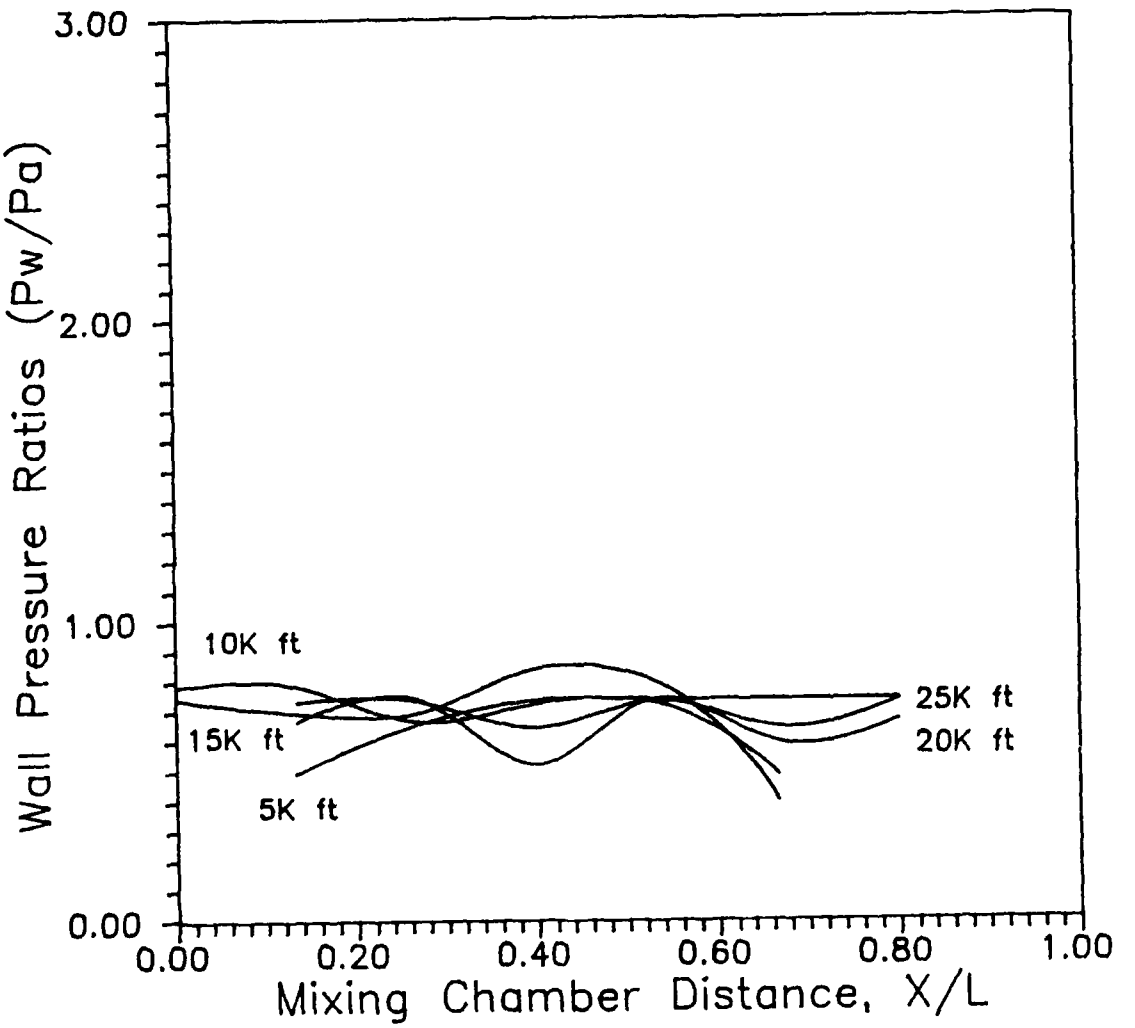

Figure 32. Wall Pressure Ratios for Low Altitude

relatively constant value of P_w/P_a between altitudes. While there are still oscillations due to the remaining shock and expansion patterns within the chamber, the pressures are generally in the 0.7 to 0.8 range of P_w/P_a. This indicates that no significant additional change in the pressure thrust term mentioned earlier would be expected in this performance regime.

Math Model

The complexity of the flow within the mixing chamber is very evident from any schlieren photograph. Figure 33 shows several variations that can be seen within the chamber at any time. Therefore, modeling this flow must be carefully considered. One basic but usually effective approach would be the application of the one-dimensional momentum equation to a control volume containing the mixing chamber. This procedure gives some idea as to the exit pressure from the chamber, exit Mach number, and possible thrust augmentation.

The control volume is shown in Figure 34. The momentum equation applied to the constant area, frictionless, adiabatic control volume is as follows:

$$\Sigma F_x = m_3U_3 - m_2U_2 - m_1U_1 = P_1A_1 + P_2A_2 - P_3A_3 \qquad (6)$$

where

ΣF_x = summation of the axial forces (lbf)

m_1 = mass flow rate of the primary flow (slugs/sec)

m_2 = mass flow rate of the secondary flow (slugs/sec)

A. LOW BACK PRESSURE

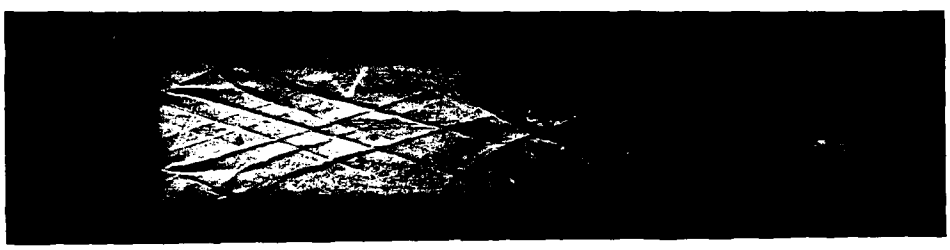

B. INCREASING BACK PRESSURE

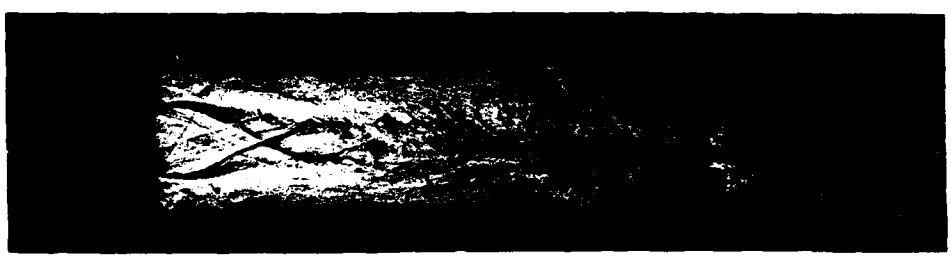

C. SEA LEVEL CONDITIONS

FIGURE 33. COMPLEX FLOW OF THE MIXING CHAMBER

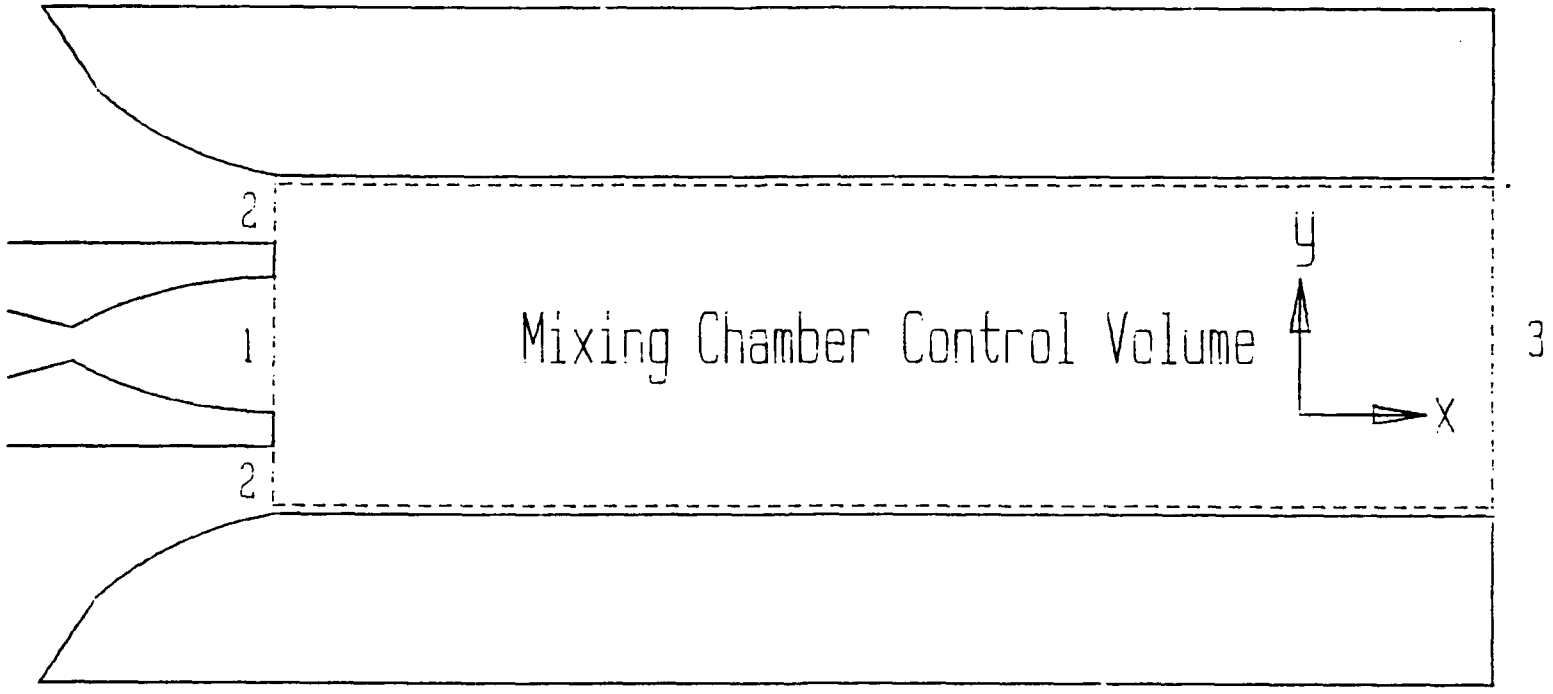

Figure 34. Control Volume for Mixing Chamber

m_3 = total mass flow rate at mixing chamber exit

= $m_1 + m_2$ (slugs/sec)

P_1 = static pressure at primary nozzle exit (psia)

P_2 = static pressure at secondary flow exit (psia)

P_3 = static pressure at mixing chamber exit (psia)

A_1 = cross-sectional area of primary nozzle exit (in^2)

A_2 = cross-sectional area of secondary flow exit (in^2)

A_3 = cross-sectional area of mixing chamber exit (in^2)

U_1 = primary nozzle exit velocity (ft/sec)

U_2 = secondary flow exit velocity (ft/sec)

U_3 = mixing chamber exit velocity (ft/sec)

The calculation starts with an assumption for P_3 and an iteration to solve for U_3. The following procedure is followed.

1) m_1 is solved using equation 5 and solving for the throat conditions of the primary nozzle.

2) m_2 is solved using equation 5 and solving for the throat conditions of the ejector.

3) m_3 is the total of m_1 and m_2

4) P_1 is solved by using equation 4 and assuming Mach 3.09 at the exit plane of the primary nozzle.

5) P_2 is solved by using equation 4 and assuming Mach 1 at the throat (or exit plane).

6) A_1 and A_2 are given by design. $A_3 = A_1 + A_2$ + the area of the base regions at the nozzle exit (0.375 inches).

7) U_1 is solved using

$$U = M(kRg_cT)^{1/2} \quad (7)$$

where

U = velocity (ft/sec)

M = Mach number

Rg_c = gas constant ($ft^2/sec^2-°R$)

= 1716

T = static temperature (°R)

The static temperature is calculated by the isentropic relationship

$$T = T_T \left(1 + \frac{k-1}{2} M^2\right)^{-1} \quad (8)$$

8) U_2 is solved using equations 7 and 8

9) U_3 is calculated using equation 6 with an assumed value for P_3.

10) With U_3, the lensity is calculated using

$$d_3 = \frac{g_c m_3 * 144}{A_3 U_3} \quad (9)$$

where

d_3 = mixing chamber exit static density (lbm/ft^3)

m_3 = mixing chamber exit mass flow rate (slugs/sec)

A_3 = mixing chamber exit cross-sectional area (in^2)

U_3 = mixing chamber exit velocity (ft/sec)

11) With d_3, the static temperature T_3 can be calculated at the exit using the perfect gas relationship

$$T_3 = \frac{P_3 * 144}{d_3 R} \qquad (10)$$

where

T_3 = mixing chamber static temperature (°R)

P_3 = mixing chamber static pressure (psia)

d_3 = mixing chamber static density (lbm/ft^3)

R = gas constant

= 53.34 (ft-lbf/lbm-°R)

12) The exit Mach number can now be calculated using equation 8 and assuming adiabatic flow through the chamber.

13) The resulting Mach number was then used in equation 7 to check the initial calculation of U_3. If they matched, the assumed value of P_3 was correct. If they did not, a new value of P_3 must be assumed and iteration accomplished until the resulting Mach number produces a velocity equivalent to the initial U_3 calculation. Tables 3 through 8 in Appendix B provide the raw data values for the calculations of the math model solutions for the selected profile.

Comparison of Math Model and Selected Profile

The selected launch profile representative of the launch schedule shown in Figure 1 is compared to the math model in Figure 35 for the ejector-rocket. An exit pressure, P_3, was calculated by the math model and compared

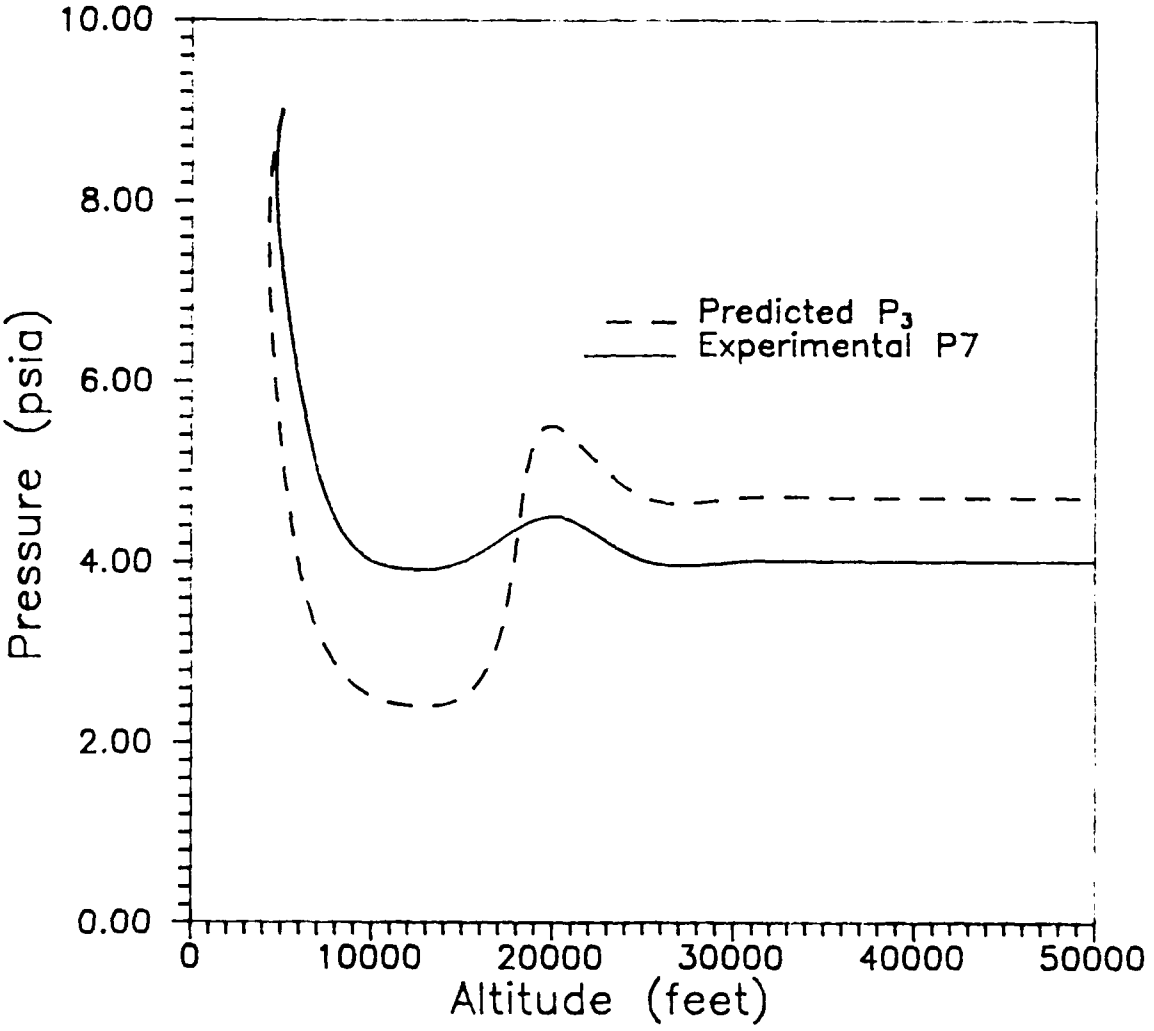

Figure 35. Comparison of Experimental Data and Math Model

to the final measured wall pressure, P7, which is assumed to equal the exit pressure. Though not totally clear why both the predicted and experimental values make the two variations in the curve, the model does reflect what the profile seems to do. While the mathematics involved in this model versus the discussion by Alperin (13) are vastly different , the variations in Figure 35, which seem to occur in three apparent flight regions (the decrease in pressure as the vehicle ascends, the transition region near 20,000 feet, and the constant exit pressure region beyond 20,000 feet), may reflect the different solutions Alperin studied. More extensive pressure measurements may confirm this possibility.

Thrust Augmentation

Predictions of ejector exit pressure and velocity from the math model provide an indication of thrust augmentation attributable to the change of momentum transfer and pressure thrust at the exit plane. Equation 1 is used to solve for the thrust of the rocket alone and, applied similarly at the ejector-rocket exit plane, permits the comparison shown in Figure 36. For the rocket-ejector, the wall pressure, P7, is assumed to be approximately equal to P_e. The curves reflect a somewhat modest but definite increase in thrust over most of the altitude range being discussed within this study. The somewhat lower thrust at 5,000 feet and, assumably, near sea level, may detract somewhat from a clear

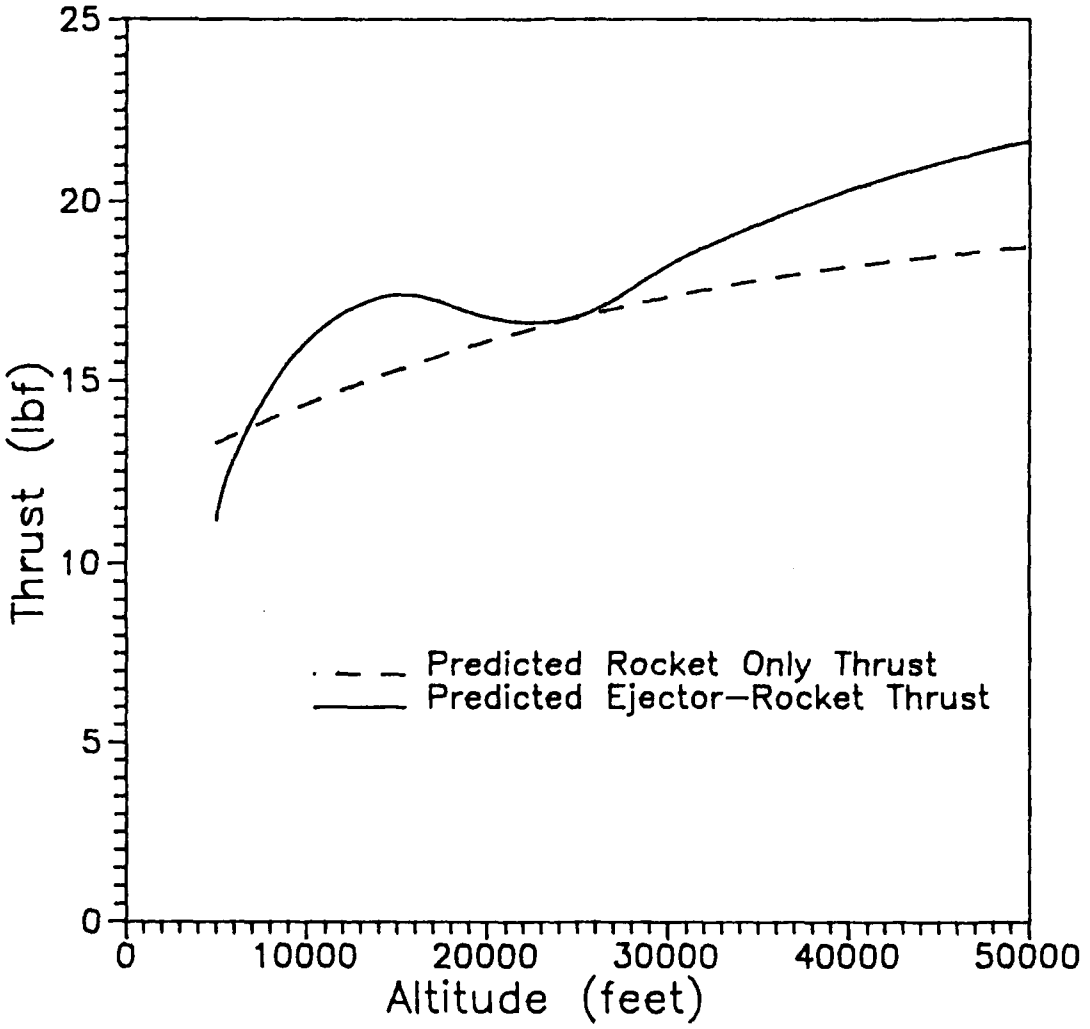

Figure 36. Thrust Comparisons of Rocket Only vs Combined Ejector–Rocket

improvement, but the curve clearly suggests the possibility of thrust augmentation over the low altitude region.

These results also must be concluded with the understanding that any supersonic drag effects from the inlet and mixing chamber, friction, and base pressure calculations have not been included in this estimation and will require further study.

VII. Conclusions

Wall pressures and flow interactions of 42 separate experimental runs were studied in the simulation of a ejector-rocket launch from sea level to 50,000 feet. The apparatus and instrumentation provided satisfactory information for this research. The results from the investigation yielded the following conclusions:

1. The wall pressures within the mixing chamber of an ejector-rocket are higher as the rocket launches from sea level and decrease during the climb. The magnitude of the pressures and the rate of decrease are dependent upon the vehicle Mach number.

2. The geometry and magnitude of the secondary flow significantly affect flow conditions of the ejector-rocket. Any angularity of the ejector secondary flow toward the primary nozzle flow causes an extraordinary amount of turbulence in the region just beyond the exit planes of the primary and secondary flows.

3. A small but definite increase in thrust may be anticipated in the overall model of the selected launch profile for the ejector-rocket model versus a rocket only launch. While this is based on a one-dimensional math model which eliminates a great deal of the internal complexity of the flow, it does provide some insight to the possible benefits that could be used to augment thrust of a rocket with an appropriately sized ejector.

VIII. Recommendations

The following recommendations are made for continuation of this work in the area of ejector-rockets:

1. The extensive fluctuations of the wall pressures received by the data acquisition system, while partly due to the extreme vibratory nature of the shocks near the transducers, tends to hamper the evaluation of the data. An analog receiver might provide less fluctuations and make the data more manageable.

2. More extensive instrumentation of the mixing chamber should be used. Such possible changes should include static pressure ports through the plexiglass walls in the nozzle exit plane, secondary flow exit plane, and mixing chamber exit plane. Additionally, a total pressure probe at the exit plane of the mixing chamber should be developed to accurately determine exit velocity. This should lead to a better determination of possible increases in thrust augmentation.

3. A definite change in the mass flow ratios is necessary. While secondary-to-primary flow ratios of 0.2 to 0.5 were used during this study, actual ratios of 4 to 5 would probably be needed in propulsion systems for future use of this arrangement. Changes would need to be made to the flow system to provide for adjustment capabilities of the primary flow as well as the secondary flow to get these mass flow ratios.

4. The optical glass viewing area should be expanded to allow for more extensive schlieren photography capabilities for both still pictures and video or film.

Appendix A: Altitude Calculations

The time the experiments were running was translated into altitude using the changes in the vacuum tank pressure, P9, which simulated the changes in altitude over the launch profile. The standard atmosphere has several layers where the temperature acts differently. These temperature changes result in distinct equations to calculate state properties at particular altitudes.

This procedure used the value for P9 and translated it into an altitude using one of the following equations (14):

Layer 1

For 0 < H < 36089.2 feet

or 14.69583 > P > 3.18253 psia

$$H = -2.804137E+02\left[\left[\frac{P * 144}{1.137193514E-11}\right]^{.19025633} - 518.69\right] \quad (11)$$

Layer 2

For 36089.2 < H < 65616.8 feet

or 3.28253 > P > 0.79410 psia

$$H = -2.080629E+04 \ln\left[\frac{P * 144}{2678.28681}\right] \quad (12)$$

Layer 3

For 65616.8 < H < 104986.9 feet

or 0.79410 > P > 0.125900 psia

$$H = 1822.688831\left[\left(\frac{P * 144}{3.80207578E+90}\right)^{-.029270236} - 353.99\right] \quad (13)$$

Layer 4

For 104986.9 < H < 154199.5 feet

or 0.125900 > P > 0.016090 psia

$$H = 6.509611E+02\left[\left(\frac{P * 144}{1.44217649E+33}\right)^{-.081956553} - 250.31\right] \quad (14)$$

Appendix B: Math Model Tabular Data

Table 3. Selected Profile Wall Pressures

ALTITUDE feet	P_1 psia	P_2 psia	P_3 psia	P_4 psia	P_5 psia	P_6 psia	P_7 psia
5000	12.23	6.0	8.0	9.0	9.0	9.0	9.0
10000	10.11	7.5	7.0	7.0	8.5	8.0	4.0
15000	8.30	6.5	6.5	5.5	6.0	6.0	4.0
20000	6.36	4.5	5.0	3.5	5.0	4.0	4.5
25000	5.46	4.0	4.0	3.5	4.0	3.5	4.0
30000	4.37	4.0	4.0	3.5	4.0	3.5	4.0
35000	3.47	4.0	4.0	3.5	4.0	3.5	4.0
40000	2.73	4.0	4.0	3.5	4.0	3.5	4.0
45000	2.15	4.0	4.0	3.5	4.0	3.5	4.0
50000	1.69	4.0	4.0	3.5	4.0	3.5	4.0

Table 4. Math Model Inputs, Rocket Nozzle Only

ALTITUDE feet	P_{T_i} psia	M_i	U_i ft/s	m_i lbm/s	A_i in^2	P_i psia
5000	110	3.09	2044	.2871	.5202	2.618
10000	110	3.09	2044	.2871	.5202	2.618
15000	110	3.09	2044	.2871	.5202	2.618
20000	110	3.09	2044	.2871	.5202	2.618
25000	110	3.09	2044	.2871	.5202	2.618
30000	110	3.09	2044	.2871	.5202	2.618
35000	110	3.09	2044	.2871	.5202	2.618
40000	110	3.09	2044	.2871	.5202	2.618
45000	110	3.09	2044	.2871	.5202	2.618
50000	110	3.09	2044	.2871	.5202	2.618

Table 5. Math Model Inputs, Secondary Flow

ALTITUDE feet	P_{T_2} psia	M_2	U_2 ft/s	$\dot{m}_2$ lbm/s	A_2 in^2	P_2 psia
5000	15	1.0	648*	.2079	.4*	7.924
10000	15	1.0	1030	.1386	.4	7.924
15000	13	1.0	1030	.1201	.4	6.868
20000	12	1.0	648*	.1663	.4*	6.339
25000	10.5	1.0	648*	.1455	.4*	5.547
30000	10.5	1.0	648*	.1455	.4*	5.547
35000	10.5	1.0	648*	.1455	.4*	5.547
40000	10.5	1.0	648*	.1455	.4*	5.547
45000	10.5	1.0	648*	.1455	.4*	5.547
50000	10.5	1.0	648*	.1455	.4*	5.547

* X-component

Table 6. Math Model Outputs

ALTITUDE feet	m_3 lbm/s	A_3 in^2	P_3 psia	U_3 ft/s	M_3
5000	.4950	1.2952	9.0	994.81	1.015
10000	.4257	1.2952	2.5	1812.00	2.29
15000	.4072	1.2952	2.5	1814.00	2.19
20000	.4534	1.2952	5.5	1303.00	1.38
25000	.4326	1.2952	4.7	1388.22	1.48
30000	.4326	1.2952	4.7	1388.22	1.48
35000	.4326	1.2952	4.7	1388.22	1.48
40000	.4326	1.2952	4.7	1388.22	1.48
45000	.4326	1.2952	4.7	1388.22	1.48
50000	.4326	1.2952	4.7	1388.22	1.48

Table 7. Thrust Calculations, Rocket Nozzle Only

ALTITUDE feet	P_a psia	m_i lbm/s	U_i ft/s	P_i psia	A_i in^2	F_i lbf
5000	12.23	.2871	2044	2.618	.5202	13.24
10000	10.11	.2871	2044	2.618	.5202	14.34
15000	8.30	.2871	2044	2.618	.5202	15.28
20000	6.36	.2871	2044	2.618	.5202	16.09
25000	5.46	.2871	2044	2.618	.5202	16.76
30000	4.37	.2871	2044	2.618	.5202	17.33
35000	3.47	.2871	2044	2.618	.5202	17.80
40000	2.73	.2871	2044	2.618	.5202	18.18
45000	2.15	.2871	2044	2.618	.5202	18.48
50000	1.69	.2871	2044	2.618	.5202	18.72

Table 8. Thrust Calculations, Ejector-Rocket

ALTITUDE feet	P_A psia	m_3 lbm/s	U_3 ft/s	P_3 psia	A_3 in^2	F_3 lbf
5000	12.23	.4950	995	9.0	1.2952	11.12
10000	10.11	.4257	1812	4.0	1.2952	16.06
15000	8.30	.4072	1814	4.0	1.2952	17.39
20000	6.36	.4534	1303	5.5	1.2952	16.73
25000	5.46	.4326	1388	4.0	1.2952	16.77
30000	4.37	.4326	1388	4.0	1.2952	18.19
35000	3.47	.4326	1388	4.0	1.2952	19.35
40000	2.73	.4326	1388	4.0	1.2952	20.31
45000	2.15	.4326	1388	4.0	1.2952	21.06
50000	1.69	.4326	1388	4.0	1.2952	21.66

Bibliography

1. Moran, J. R. An Experimental Study of Clustered Nozzles with Variable Shrouds. MS Thesis AFIT/GA/AA/85D-1. School of Engineering, Air Force Institute of Technology (AU), Wright-Patterson AFB, OH, December 1985.

2. Rodgers, D. C. Investigation of Shrouded Nozzle Exit Pressure Changes. MS Thesis AFIT/GA/AA/86D-15. School of Engineering, Air Force Institute of Technology (AU), Wright-Patterson AFB, OH, December 1986.

3. Maxwell, J. A. An Experimental Study of a Rocket Ramjet Nozzle Cluster. MS Thesis AFIT/GA/AA/87M-3. School of Engineering, Air Force Institute of Technology (AU), Wright-Patterson AFB, OH, March 1987.

4. Wesling, T. R. An Experimental Investigation of Rocket Ramjet Nozzle Assembly Base Pressures. MS Thesis AFIT/GA/AA/87D-9. School of Engineering, Air Force Institute of Technology (AU), Wright-Patterson AFB, OH, December 1987.

5. Shapiro, A. H. The Dynamics and Thermodynamics of Compressible Fluid Flow. Vol. 1. New York: John Wiley and Sons, Inc., 1964.

6. Gaines, L.M. and others. "Shuttle Performance: Lessons Learned," Launch Vehicle Aerodynamics Flight Test Results. NASA-CP 2283, Part 1, 1983.

7. Sutton, G. P. and D. Ross. Rocket Propulsion Elements (Fourth Edition). New York: John Wiley and Sons, Inc., 1976.

8. Daley, D. H. "A Nozzle Operating Diagram," Bulletin of Mechanical Engineering Education, Vol. 6, pp. 245-257. Pergamon Press, 1967.

9. Hill, P. G. and C. R. Peterson. Mechanics and Thermodynamics of Propulsion. Reading, Massachusetts: Addison-Wesley, 1970.

10. Keenan, J. H. and Neumann, E. P. "A Simple Air Ejector," Journal of Applied Mechanics, 64: A-75-A-84, (July 1942).

11. Amatucci, V. A. and others. "Pressure Recovery in a Constant-Area, Two-Stream Supersonic Diffuser," AIAA Journal, 20: 1308-1309 (September 1982).

12. Dutton, J. C. and others. "A Theoretical and Experimental Investigation of the Constant Area, Supersonic-Supersonic Ejector," AIAA Journal, 20: 1392-1400 (October 1982)

13. Alperin, M. and Wu, J. J. High Speed Ejectors, September 1977-December 1978. Contract F33615-77-C-3160. Van Nuys, CA: Flight Dynamics Research Corporation, May 1979 (AD-A073378)

14. Fowler, Wallace T. Class handout distributed in Aero 367L, Flight Test Engineering, School of Engineering, University of Minnesota, MN, October 1983.

Vita

Captain Christopher A. Seaver [redacted] In May 1980 he received the degree of Bachelor of Science in Aeronautical Engineering from the United States Air Force Academy. Upon graduation, he attended pilot training at Columbus AFB, Mississippi and received his wings in August 1981. He then served as an instructor pilot with the 50th Flying Training Squadron and as an academic instructor with the 14th Student Squadron at Columbus. From there, he went to Randolph AFB, Texas where he served as a pilot instructor trainer and standardization and evaluation pilot for the 560th Flying Training Squadron and the 12th Flying Training Wing. Captain Seaver entered the Air Force Institute of Technology in May of 1987.

[redacted]

UNCLASSIFIED

SECURITY CLASSIFICATION OF THIS PAGE

REPORT DOCUMENTATION PAGE

Form Approved OMB No. 0704-0188

1a. REPORT SECURITY CLASSIFICATION: UNCLASSIFIED	1b. RESTRICTIVE MARKINGS
2a. SECURITY CLASSIFICATION AUTHORITY	3. DISTRIBUTION/AVAILABILITY OF REPORT: Approved for public release; distribution unlimited
2b. DECLASSIFICATION/DOWNGRADING SCHEDULE	
4. PERFORMING ORGANIZATION REPORT NUMBER(S): AFIT/GAE/AA/88D-33	5. MONITORING ORGANIZATION REPORT NUMBER(S)
6a. NAME OF PERFORMING ORGANIZATION: School of Engineering; 6b. OFFICE SYMBOL (If applicable): AFIT/ENY	7a. NAME OF MONITORING ORGANIZATION
6c. ADDRESS (City, State, and ZIP Code): Air Force Institute of Technology, Wright-Patterson AFB OH 45433-6583	7b. ADDRESS (City, State, and ZIP Code)
8a. NAME OF FUNDING/SPONSORING ORGANIZATION; 8b. OFFICE SYMBOL (If applicable)	9. PROCUREMENT INSTRUMENT IDENTIFICATION NUMBER
8c. ADDRESS (City, State, and ZIP Code)	10. SOURCE OF FUNDING NUMBERS: PROGRAM ELEMENT NO. / PROJECT NO. / TASK NO / WORK UNIT ACCESSION NO.

11. TITLE (Include Security Classification)
EJECTOR EFFECTS ON A SUPERSONIC NOZZLE AT LOW ALTITUDE AND MACH NUMBER

12. PERSONAL AUTHOR(S)
Christopher A. Seaver, Capt, USAF

13a. TYPE OF REPORT	13b. TIME COVERED	14. DATE OF REPORT (Year, Month, Day)	15. PAGE COUNT
MS Thesis	FROM _____ TO _____	1988 December	104

16. SUPPLEMENTARY NOTATION

17. COSATI CODES			18. SUBJECT TERMS (Continue on reverse if necessary and identify by block number)
FIELD	GROUP	SUB-GROUP	Ejectors, Supersonic Nozzles
21	08		

19. ABSTRACT (Continue on reverse if necessary and identify by block number)

Thesis Advisor: Dr. William C. Elrod, Professor
Department of Aeronautics and Astronautics

ABSTRACT ON BACK

Approved for release in accordance with AFR 190-1
[signature]
12 Jan 1989

20. DISTRIBUTION/AVAILABILITY OF ABSTRACT	21. ABSTRACT SECURITY CLASSIFICATION
☐ UNCLASSIFIED/UNLIMITED ☒ SAME AS RPT. ☐ DTIC USERS	UNCLASSIFIED
22a. NAME OF RESPONSIBLE INDIVIDUAL: Dr. William C. Elrod, Professor	22b. TELEPHONE (Include Area Code): (513) 255-3517; 22c. OFFICE SYMBOL: AFIT/ENY

DD Form 1473, JUN 86 — Previous editions are obsolete.